Metal Sulfide Photocatalysts for Lignocellulose Valorization

Xuejiao Wu, Shunji Xie,* Haikun Zhang, Qinghong Zhang, Bert F. Sels,* and Ye Wang*

Prof. S. Xie, H. Zhang, Prof. Q. Zhang, Prof. Y. Wang
State Key Laboratory of Physical Chemistry of Solid Surfaces,
Collaborative Innovation Center of Chemistry for Energy Materials,
National Engineering Laboratory for Green Chemical Productions of Alcohols, Ethers and Esters,
College of Chemistry and Chemical Engineering,
Xiamen University,
Xiamen 361005, China
E-mail: shunji_xie@xmu.edu.cn; wangye@xmu.edu.cn

Dr. X. Wu, Prof. B. F. Sels
Centre for Sustainable Catalysis and Engineering,
Faculty of Bioscience Engineering,
KU Leuven,
Heverlee 3001, Belgium
E-mail: bert.sels@kuleuven.be

Abstract

Transition metal sulfides are an extraordinarily vital class of semiconductors with a wide range of applications in the photocatalytic field. A great number of recent advances in photocatalytic transformations of lignocellulosic biomass, the largest renewable carbon resource, into high-quality fuels and value-added chemicals have been achieved over metal sulfide semiconductors. This Progress Report highlights the progress and breakthroughs in metal sulfide-based photocatalytic systems for lignocellulose valorization with an emphasis on selective depolymerization of lignin and oxidative-coupling of some important bio-platforms. The key issues that control reaction pathways and mechanisms are carefully examined. The functions of metal sulfides in the elementary reactions, including C−O bond cleavage, selective oxidations, C−C coupling and C−H activation, are discussed to offer insights to guide the rational design of active and selective photocatalysts for sustainable chemistry. The prospects of sulfide photocatalysts in biomass valorization are also analyzed and briefly discussed.

1. Introduction

Petroleum is currently the primary energy and carbon resource that sustains the development of our modern society, while diminishing reserves and certainly the adverse environmental impacts of crude oil have stimulated the exploitation of more sustainable solutions. In fact, a gradual transition from petroleum to renewable substitutions, such as solar energy and wind power, has been taking place in the energy matrix for decades. However, petroleum remains to be the major supply of carbon-based fuels and chemicals, and the pursue of clean-carbon-solution is one of the greatest challenges for our society.[1-3] The utilization of biomass, which is the most abundant renewable carbon resource with easy accessibility, can greatly alleviate the reliance on fossil feedstocks. In particular, the selective transformations of the underutilized and inedible lignocellulosic biomass to provide renewable fuels and chemicals have attracted a great deal of attention in science.[4-6]

Lignocellulose, the most abundant form of biomass, is a complex and rather recalcitrant feedstock comprising three major components, i.e., 15-30% lignin, 40-60% cellulose, 10-40% hemicellulose.[7] Lignin is an irregular aromatic polymer, while cellulose and hemicellulose are polysaccharides. All three components of lignocellulose are macromolecules with high functionality, and thus they represent superior feedstocks for the production of high-value functionalized chemicals and high-carbon-number products.[6-8] Given a great number of pathways to different products are possible for these highly functionalized lignocellulose-based molecules, the selective transformation to the target product is the crucial key and a formidable challenge. Conventional approaches for the conversion of lignocellulose, such as pyrolysis and hydrogenolysis, usually require severe operational conditions and thus lead to low product selectivity.[5] Photocatalysis that can be performed under mild and environmental-benign conditions has emerged as a promising tool for selective transformations of lignocellulose.[9-11]

Photocatalysis has been recognized as a useful strategy for selective transformations in organic synthesis for a few decades.[10] The unique ability of photocatalysis in generating redox species or reactive intermediates under mild conditions provides new possibilities that go beyond the conventional thermocatalysis. The photo-generated redox species, e.g., charge carriers or chemicals in photo-excited states, with sufficient redox potentials can drive the thermodynamically unfavorable reactions at room temperature. This may result in the occurrence of novel reactions circumventing thermodynamic limitations. Reactive intermediates like radicals can be easily generated under mild conditions, and the subsequent reactions related to these reactive intermediates are usually fast, which may accelerate kinetically difficult reactions. Selective photocatalysis can be realized by the control of redox species or reactive intermediates. Take semiconductor-based photocatalysis as an example, strategies such as composite construction and doping have been devised to tune the redox ability of the photo-generated charge carriers, and the nature of radical intermediates can be manipulated by changing the reaction conditions and by the surface properties of the catalyst.[9, 11, 12] These characteristics of photocatalysis enable the selective transformation of the multifunctional lignocellulose-based feedstock to target products under mild conditions, which has received increasing research interest.[4, 13-18]

In the past decade, some homogeneous photocatalysts, including transition metal complexes (e.g., polypyridyl complexes of ruthenium and iridium) and organic photoredox catalysts (e.g., acridiniums and phenothiazines), have been used for the valorization of biomass.[4,13] The long lifetimes and the large redox window of the excited states of these homogenous catalysts enable them to successfully catalyze a variety of redox reactions for biomass valorization.[19] However, homogenous photocatalysts are usually sensitive to the reaction environment, tolerant only to limited functional groups, and may undergo deactivation under the complicated reaction environment for biomass conversions.[20] Therefore, although many homogenous photocatalysts have shown good performances in for

instance the cleavage of C−O or C−C bond in lignin model compounds, few of them have succeeded in the transformation of extracted or native lignin.[4] Moreover, the products from the conversion of biomass normally are a mixture of organic compounds, rendering the separation and recycling of homogenous photocatalysts from products highly challenging. Immobilization of homogeneous catalysts onto solid supports can solve these problems to some extent.

As compared to homogeneous photocatalysts, a heterogeneous photocatalyst usually shows better compatibility to the reaction environment and higher long-term stability, and the catalyst can be separated from organic products and recycled more easily.[21] Because of these advantages, heterogeneous semiconductors have been widely investigated for photocatalytic valorization of biomass.[4] The semiconductor-based photocatalysis was first used for H_2 production from raw lignocellulosic biomass or bio-platforms, and metal oxides were found to be efficient photocatalysts for H_2 production.[16] In this process, lignocellulosic biomass or bio-platforms functioned as hole scavengers and CO_2 was typically produced as the major by-product.[22] Recently, many non-oxide semiconductors have been studied for the selective conversion of lignocellulose related chemicals into high-value products. Among the non-oxide semiconductors, metal sulfides have shown promising performances in selective valorization of biomass and have attracted much research attention.

Metal sulfides are an outstandingly dynamic class of semiconductor photocatalysts.[23−25] Cations used for constructing sulfide semiconductors are mostly metals with d^{10} configuration, such as Zn, Cd, Cu, Ag, In and Sn (Figure 1a).[25] In metal sulfides, the atomic orbitals of cations and S^{2-} hybridize into a great number of closely spaced molecular orbitals, which constitute the conduction bond (CB) and valence band (VB). The band edges (i.e., the bottom of the CB and the top of the VB) are mostly features of the outermost orbitals of the atoms. The atomic energy of the outermost orbitals (np) for the elementals in group VIA generally increases on going down the group (Figure 1b, where the energies are from the NIST

database). It is worth mentioning that the atomic orbital energies of chalcogenide p (S, Se, Te) are close to each other but not to that of O $2p$, and this distinguishes metal oxides from metal chalcogenides (Figure 1b). For non-transition metal sulfides, the CB edges are primarily derived from metal s or p orbitals, whereas VB edges are mainly derived from S $3p$ orbitals.[26] For the transition metal sulfides, metal d states can also be present near metal s/p orbitals or S $3p$ orbitals and can hybridize to the CB or VB edges.[27, 28] Figure 1c displays an illustrative electronic structure of CdS.[29] Nevertheless, most metal sulfide semiconductors are with negative CB, suggesting a strong reduction ability, similar to metal oxides. In addition, most metal sulfides possess weaker oxidation ability than metal oxides because of the higher VB position contributed from the S $3p$ orbital, relative to the O $2p$ orbital (Figure 1d). Therefore, metal sulfides usually have a strong reduction ability, relatively soft oxidation ability, and narrow bandgaps.[30, 31]

Because of the more localized nature of the O $2p$ state as compared to the S $3p$ state, the hole carriers of metal oxides usually have a heavier effective mass than those of metal sulfides,[32] indicating higher hole mobility of metal sulfides for better charge transfer. Further, many metal oxides possess wide bandgaps, and thus can only use UV light, which constitutes only 3% of the solar light. In contrast, a lot of metal sulfides can absorb visible light, and thus metal sulfides usually have a wider solar light-responsive spectrum as compared to metal oxides (Figure 1d).
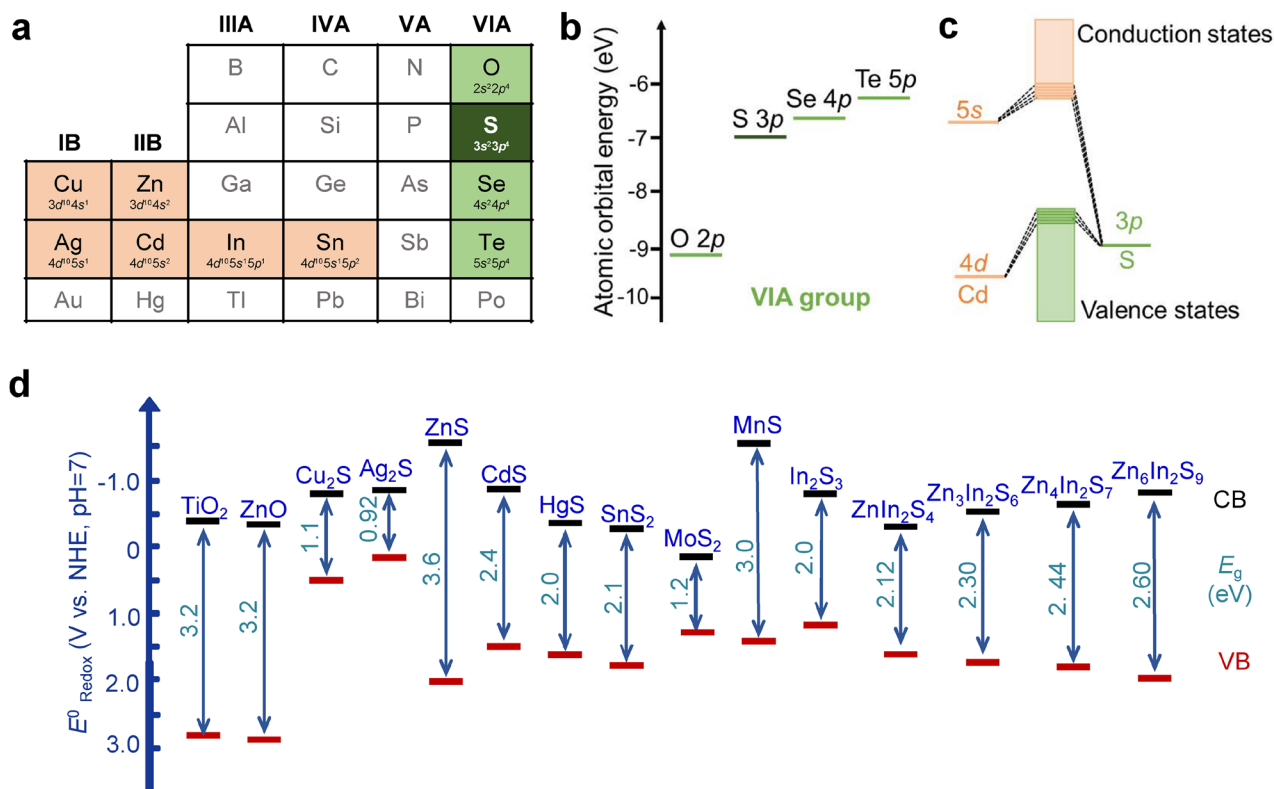
Figure 1. a) Part of the Periodic Table. Metals constructing most of the metal sulfides are highlighted with an orange background, and O, S, Se, Te in group VIA are highlighted with a green background. b) Atomic orbital energies of O, S, Se, Te. The values are from the NIST database. c) Illustrative electronic structure of CdS. Only the major contribution from atomic orbitals to the band edges is displayed. d) Band positions of some typical oxides and sulfides. The values are from Xu et al.[26] and Lin et al.[31].

The genealogy of the reported sulfide photocatalysts includes binary sulfides (e.g., CdS, ZnS) and multinary sulfides (e.g., $Zn_{1-x}Cd_xS$, $Zn_mIn_2S_{m+3}$).[23-25, 33] CdS, which has a bandgap of ~2.4 eV and is visible-light ($\lambda < 520$ nm) responsive, is probably the most investigated metal sulfide photocatalyst for the valorization of biomass. Notably, the photophysical and photocatalytic properties of CdS can be tuned by controlling its structural parameters such as phases, sizes, and morphologies.[33, 34] CdS has two common crystalline phases, i.e., wurtzite and zinc blende phases. As compared to zinc blende CdS, the wurtzite CdS usually shows

better photocatalytic activities. This can be ascribed to the anisotropy structure and the smaller effective mass of photo-generated charge carriers of the wurtzite phase.[35] The size of CdS can be easily manipulated by changing the synthetic conditions or synthetic materials. CdS particles with sizes smaller than CdS Bohr exciton diameter (6.4 nm) in three dimensions are known as quantum dots (QDs) because of the quantum confinement effect. QDs possess many distinct properties such as abundant surface sites and tunable redox potentials. CdS QDs have recently been discovered as efficient catalysts in a number of photocatalytic systems.[33] CdS nanomaterials can be synthesized in various morphologies, such as nanorods, nanosheets and flower-like or tree-like shapes. Among the CdS nanomaterials with different morphologies, the one-dimensional (1D) CdS nanorods have attracted considerable attention because of the unique structural properties, i.e., quantum confinement in the radial direction and bulk-like feature in the axial direction, which facilitate the fast generation and separation of photo-generated excitons.[36]

ZnS, another typical metal sulfide with a wider bandgap of ~3.6 eV, can only absorb UV light (λ < 340 nm) and is less investigated than the visible-light responsive CdS.[24,34] The bandgap of ZnS can be narrowed by incorporating other metal cations to form multinary sulfides that contain more than one metal cations. The band structure of multinary sulfides can be manipulated by changing their composition and stoichiometry, enabling a wide light-responsive spectrum and tunable redox potential. An example of the composition-controlled band structure of $Zn_mIn_2S_{m+3}$ is illustrated in Figure 1d.[23] Further, the phase, size, and morphology of multinary metal sulfides may be manipulated by changing their composition or stoichiometry, which can be performed in the synthetic step.[37] Therefore, metal sulfides with great variability have found a wide range of applications in photocatalytic field. Recently, metal sulfides have also been identified as promising photocatalytic materials for selective transformation of lignocellulosic biomass or lignocellulose-derived bio-platforms.

Although several reviews have been published on the recent advances in the field of photocatalytic transformations of lignocellulose,[4, 13-18] no review article has been focused on summarizing and analyzing the metal sulfide-based photocatalytic systems for the valorization of lignocellulosic biomass. This contribution, which would fill this gap in literature, is devoted to providing an overview of recent progress in the field of photocatalytic transformations of lignocellulosic biomass over metal sulfide semiconductors (Figure 2). Selective transformations of biopolymers into value-added products usually involve two consecutive catalytic steps,[7] i.e., the depolymerization of macromolecules to small platform chemicals and the down-stream upgrading of bio-platforms to targeted products. The cleavage of target C−O or C−C bonds and the selective transformation of specific functional groups with other functional groups kept intact are key challenging tasks for the selective depolymerization and upgrading. The following advances will mainly be highlighted in the present article: i) metal sulfides are found as efficient catalysts in selective cleavage of C−O bonds in lignin; ii) metal sulfide quantum dots (QDs) can break C−O or C−C bonds in raw lignocellulosic biomass effectively; iii) high selectivities in the oxidation of bio-platforms to produce carbonyls or carboxyls are achieved over metal sulfide semiconductors; and iv) several metal sulfide-based photocatalytic systems demonstrate unique performances in coupling to produce high-carbon-number chemicals or diols and selective amination to produce amino acids (Figure 2). The reaction mechanisms for these transformations will be discussed in detail. The functions of metal sulfides in the elementary reaction steps, i.e., C−H activation, C−O cleavage, and C−C coupling, will be carefully examined, and the underlying fundamentals for the superiority of metal sulfide semiconductors will be analyzed and discussed. The structure-performance relationships of sulfide semiconductors for biomass valorization provided in this article may help to guide the rational design of efficient photocatalysts for green chemistry.
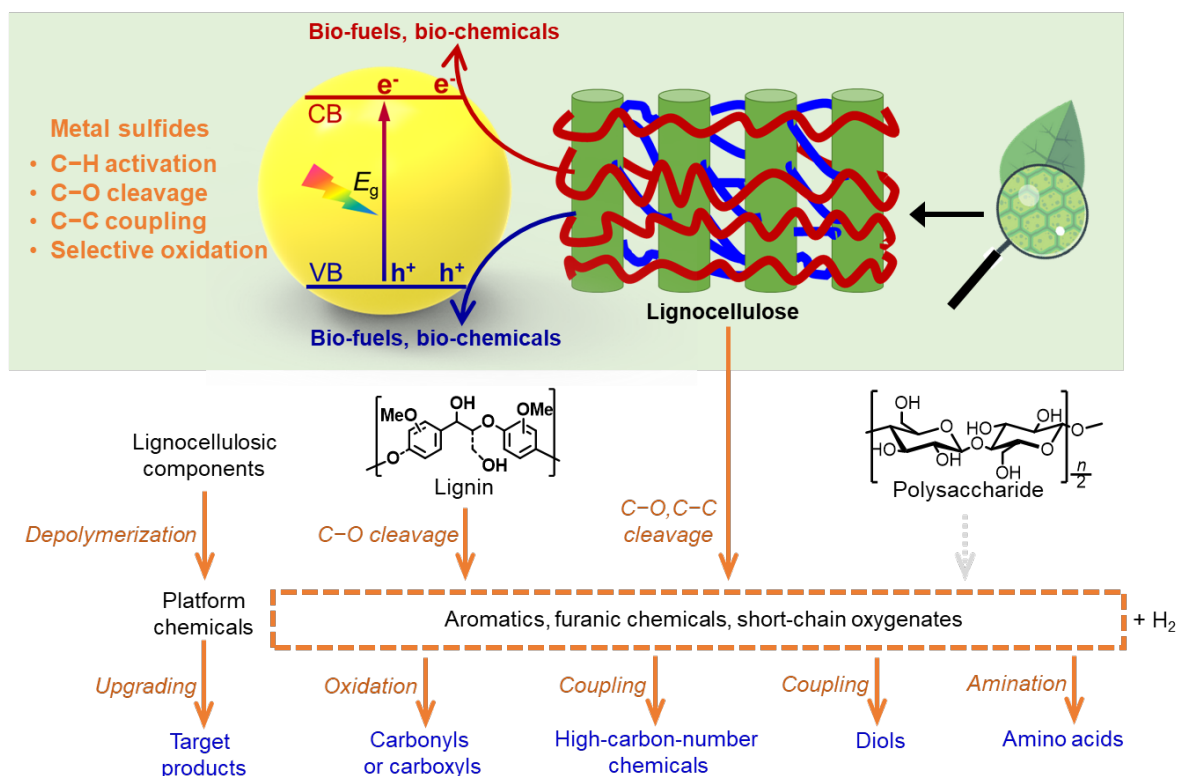
Figure 2. Photocatalytic valorization of lignocellulosic biomass over metal sulfides involved in this article.

2. Depolymerization

Current studies of metal sulfide-based photocatalytic depolymerization of biomass mainly focus on the transformations of lignin to provide aromatic monomers as products.[4, 13-18] Although being the largest resource of renewable aromatics, lignin remains poorly utilized and is commonly either released as waste or burnt to generate power.[38] The recalcitrance of chemical linkages and the interwinding of bonding motifs render the production of aromatics from lignin one of the most challenging tasks for biomass valorization.[39] Photocatalytic depolymerization of lignin by selective cleavage of interconnected C−O or C−C bonds to produce aromatic compounds has received intensive attention.[4, 13-18] A number of metal sulfide semiconductors have been reported with unique performances in photocatalytic depolymerization of lignin by selective cleavage of C−O bonds. Direct conversion of raw lignocellulose to

produce chemicals or fuels without pre-fractionation has emerged as an important research direction in the field of biomass valorization.[40, 41] Several recent advances in photocatalytic conversions of raw lignocellulosic biomass have been achieved over metal sulfide QDs.

2.1. Depolymerization of Lignin by Selective C−O Bond Cleavage

Lignin is an irregular polymer composed of *p*-propylphenols as building blocks, which are connected by C−O (e.g., β-O-4 and α-O-4) bonds and C−C (e.g., β-5 and 5-5) bonds (Figure 3).[42] Amongst different linkages in lignin, β-O-4 constitutes the most frequent motif with the abundance varying from 43% to 65% for lignin in natural lignocellulosic biomass,[43] and this number may increase to as high as 89% for bioengineered lignin.[44] Selective cleavage of β-O-4 bond is the key to depolymerization of lignin to produce aromatic monomers. The C_β−O in lignin β-O-4 motif possesses a bond dissociation energy (BDE) of 54-72 kcal mol^{-1}.[45] The oxidation of C_α−OH in β-O-4 motif to C_α=O can substantially reduce the BDE of C_β−O bond, and thus facilitate the cleavage of the C_β−O bond. Take a typical dimeric lignin β-O-4 model, i.e., 2-phenoxy-1-phenylethanol (PP-ol), as an example; the oxidation of its C_α−OH to produce 2-phenoxy-1-phenyl-ethanone (PP-one) can reduce the BDE of C_β−O bond from 55 to 47 kcal mol^{-1}.[46] A two-step method by using this pre-oxidation followed by C_β−O bond cleavage has been proven to be useful in thermocatalytic systems for selective depolymerization of lignin.[47] However, expensive oxidants and additional acids or reductants are typically required for the pre-oxidation and the bond-cleavage steps, respectively, in thermocatalytic system.[47, 48] Recent studies have demonstrated that photogenerated holes and electrons can replace the stoichiometric oxidants and reductants required for accelerating β-O-4 bonda cleavage.
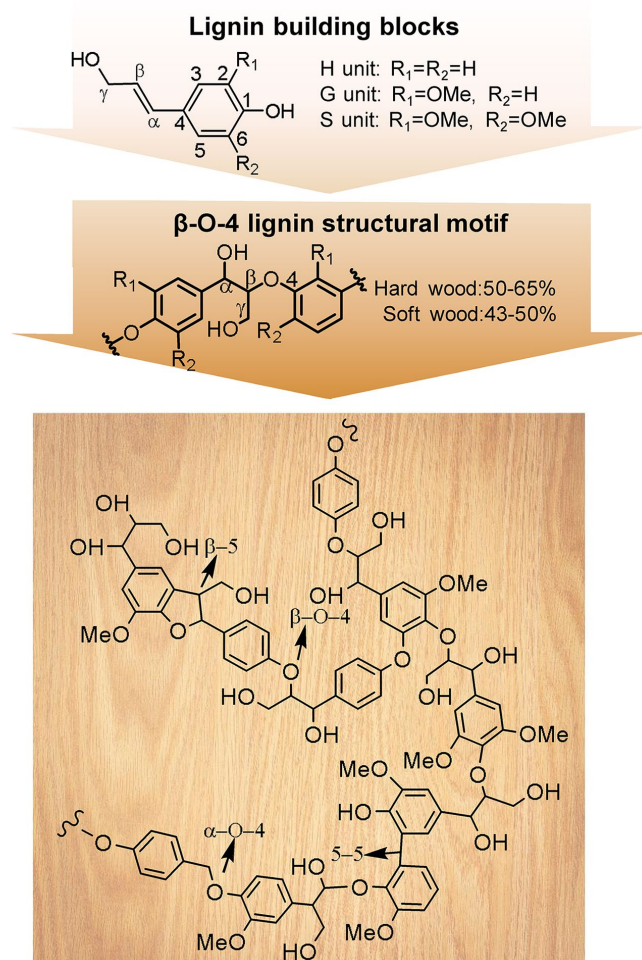
Figure 3. Chemical structures of lignin building blocks, structural illustration of lignin β-O-4 linkage and a representative fragment of lignin.

Stephenson and co-workers introduced a Ir polypyridyl complex photocatalyst into the two-step method for the conversion of lignin model compounds.[49] The first step, i.e., the pre-oxidation of C_α−OH to C_α=O, was performed by a thermocatalytic approach. The second step, i.e., the photocatalytic reduction to cleave the C_β−O bond in β-O-4 linkage, was accomplished by the Ir polypyridyl complex photocatalyst. Besides the Ir polypyridyl complex, several other photocatalysts such as π-conjugated porous organic frameworks were also found to be efficient for the cleavage of β-O-4 linkage in the second step.[50] However, the two-step method usually requires the presence of sacrificial reagents (such as diisopropylethylamine)

and the separation of the oxidized product from the first step for subsequent bond cleavage is tedious.

One-pot photocatalytic breaking of β-O-4 linkage through first oxidation of $C_\alpha H-OH$ by holes to produce ketone intermediates, followed by reductive cleavage of $C_\beta-O$ bond was realized over $ZnIn_2S_4$[51] and Ni/CdS nanosheet[52]. Mechanistic studies revealed that the oxidation of the alcoholic group ($C_\alpha H-OH$) by holes delivered ketone intermediates and protons, which were then reduced by electrons to hydrogen adsorbed on the surface of the catalyst. The hydrogen adsorbed on the surface could reductively break the $C_\beta-O$ bond in the β-O-4 ketone intermediate. This reaction pattern is also known as self-transfer hydrogenolysis, because the hydrogen generated by the oxidative dehydrogenation of $C_\alpha H-OH$ can be further used for the cleavage of the $C_\beta-O$ bond. In this case, the catalyst act as a hydrogen pool for the self-transfer hydrogenolysis process (Figure 4, left panel). It is interesting that for Ni/CdS nanosheets, the solvent plays a key role in tuning the selectivity. When the solvent was pure CH_3CN, PP-ol was oxidatively dehydrogenated to the corresponding ketone, i.e., PP-one. This might be attributed to the high H_2 evolution ability of the surface metallic Ni co-catalyst, which could abstract the hydrogen atom on the surface for the production of H_2. With electrons being consumed for H_2 evolution, PP-ol was oxidized by holes to PP-one in pure CH_3CN. Bond cleavage could only proceed in an alkaline solvent, in which a thin layer of metallic Ni surface was oxidized to $Ni(OH)_2$ or NiO_x. The oxidized Ni was a poorer H_2 evolution catalyst, and thus the absorbed hydrogen would instead participate in the cleavage of $C_\beta-O$ bond.[52]

Recently, Wang and co-workers found that CdS NPs with a cubic zinc blende structure was highly active and selective for the cleavage of $C_\beta-O$ bond in PP-ol under visible-light irradiation, producing acetophenone and phenol as the two predominant products.[46] Experimental and computational studies have pointed out a new electron-

hole coupled (EHCO) photoredox mechanism for C−O bond cleavage based on a C_α radical intermediate (Figure 4, right panel), and this is different from the previous two-step mechanism involving the C_α=O intermediate. More specifically, the C_α−H bond of PP-ol firstly breaks via the oxidative dehydrogenation (ODH) process to form a C_α radical upon oxidation by holes. The valence band maximum (VBM) of CdS (1.7 V vs SHE) has a more positive potential than the ODH potential for C_α−H bond (1.1 V vs SHE), and this ensures that the hole has sufficient oxidation capability of oxidizing PP-ol into the C_α radical. Here, the ODH potential for the C_α−H bond refers to the potential that is required for the oxidative dehydrogenation of PP-ol into C_α radical on CdS (110) surface, and its value can be readily calculated from the free energy change obtained by DFT calculations. The BDE of C_β−O bond decreases remarkably from 55 kcal mol^{-1} in PP-ol to 7.8 kcal mol^{-1} in C_α radical. The very low BDE of C_β−O bond in the C_α radical intermediate contributes to the high activity and selectivity of the photocatalytic system.[46] By accepting an electron from the CdS surface, the C_α radical undergoes facile β-O-4 bond breaking, spontaneously forming acetophenone and a phenoxy anion. The calculated reduction potential of this process is -0.21 V vs SHE, lower than the conduction band minimum (CBM) of CdS (-0.7 V vs SHE), indicating that the photogenerated electrons can readily drive the reductive cleavage of β-O-4 bond in the C_α radical (Figure 4, right panel).[46] In some early studies, the C_α radical was also found as an intermediate for the slow degradation of the residual lignin in pulp paper by photolysis, resulting in the undesirable photo-yellowing of paper. Several reports have illustrated that the generation of C_α radicals can be accelerated in the presence of H-atom abstracting species.[53, 54] The formation of C_α radical over zinc blende CdS likely proceeds through direct H-atom abstraction. However, the hole transfer followed by deprotonation may also result in C_α radical. Further studies are needed to clarify the detailed pathway for C_α radical formation and provide in-depth mechanistic insights.
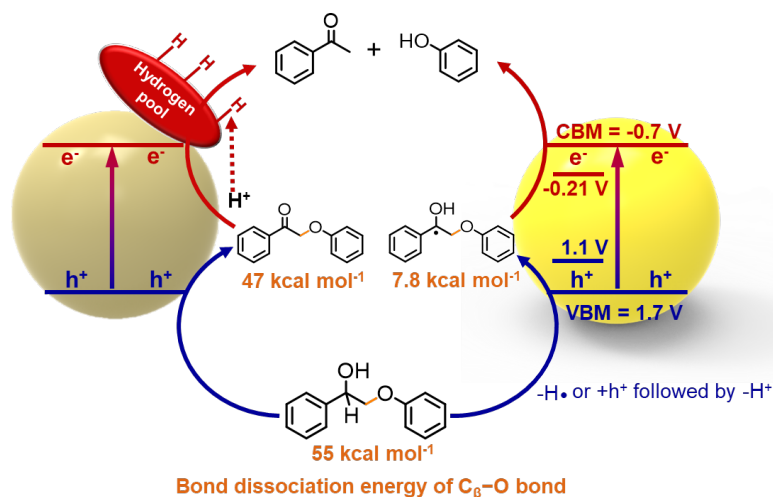
Figure 4. Proposed mechanisms for photocatalytic fragmentation of PP-ol via self-hydrogen transfer hydrogenolysis through a ketone intermediate (left panel)[51] and electron-hole coupled (EHCO) photoredox through a C_α radical intermediate (right panel)[46].

Yoo et al. found that Ag^+-exchanged wurtzite CdS could catalyze the cleavage of various lignin β-O-4 models.[55] By conducting a series of control experiments and radical-trapping studies, the authors further illustrated that the bond cleavage proceeded through C_α radical intermediate, similar to that proposed over zinc blende CdS.[46] Increasing the exchange degree of Ag^+ from 0 to 2% significantly enhanced the catalytic activity of wurtzite CdS. The Ag^+-exchanged domains could dramatically shift the Fermi level of CdS and thus contribute to the faster charge transfer, leading to the enhanced photocatalytic performance. Further, as indicated by high-resolution photoemission spectroscopy studies, the Ag^+ exchange could increase the H^+ affinity of the surface sulfide ions, and this might accelerate the dehydrogenation step to produce C_α radical.[55]

A series of $Zn_mIn_2S_{m+3}$ (m = 1-6) semiconductors synthesized by a low-temperature hydrothermal method were tested for the conversion of PP-ol.[31] All the

$Zn_mIn_2S_{m+3}$ samples displayed aggregative nanosheet morphology with a multilayer structure, and these materials had lattice fringes with an interplanar spacing of 0.32 nm, corresponding to the (102) crystallographic plane (Figure 5a). The energy-band structures of $Zn_mIn_2S_{m+3}$ could be tuned by controlling the atomic ratio of Zn to In (Figure 5b). On increasing the value of m from 1 to 6 in $Zn_mIn_2S_{m+3}$, the CBM was shifted to a more negative position, i.e., from −0.47 to −0.61 V, and the VBM was shifted to a more positive position, i.e., from 1.65 to 1.99 V. The bandgap energy gradually increased from 2.12 to 2.60 eV (Figure 5b). Among the series of $Zn_mIn_2S_{m+3}$ (m = 1-6) semiconductors, $Zn_4In_2S_7$ was found to be the best photocatalyst for the cleavage of β-O-4 bond in PP-ol under visible-light irradiation, probably because of its balanced light-harvesting ability and redox capability, affording over 80% phenol and acetophenone yields within 4 h (Figure 5b).[31] The $Zn_4In_2S_7$ photocatalyst could also efficiently drive the depolymerization of Organosolv birch lignin under visible-light irradiation. After reaction for 24 h, the color of dissolved Organosolv birch lignin changed from yellow brown to light yellow, and this may be indicative of the reduced molecular weight of the substrate (Figure 5c). Approximately 85% of β-O-4 bonds in Organosolv birch lignin were cleaved, providing an 18.4% yield of *p*-hydroxyl acetophenone derivatives as monomeric products.[31] The ratio of S units to G units in the monomer product was 3.2, which was close to that in the original lignin (2.8).

Control experiments with different substrates pointed out that the cleavage of the C_β−O bond mainly proceeded by the mechanism via C_α radical. The mechanism via C_α=O intermediate might also occur, but only as a minor contributor.[31] Moreover, the authors proposed that the thiol groups (−SH) on the surface of sulfide semiconductors were the active center for the activation of the C_α−H bond to produce the C_α radical under light irradiation. Different amounts of bromide derivatives, which were inhibitors of −SH groups, were used to treat $Zn_4In_2S_7$ in cyclohexane solution. The

catalytic performance of the treated $Zn_4In_2S_7$ sample decreased with an increase in the amount of bromide derivatives. When the devitalized $Zn_4In_2S_7$ was further treated in NaSH aqueous solution to remove bromide derivatives and regenerate −SH groups, the catalytic activity of the $Zn_4In_2S_7$ catalyst was nicely restored (Figure 5d). These results suggest that the −SH group on metal sulfide surfaces may be responsible for selective activation of the C_α−H bond to form a C_α radical intermediate.[31] It is of interest to mention that the combination of a homogeneous catalyst, $[Ir(ppy)_2dtbpy]PF_6$, with $HSCH_2CO_2Me$, a thiol, as a co-catalyst can also catalyze the cleavage of C_β−O bond in the absence of a sacrificial reagent.[56] In this system, the function of thiol is to activate the C_α−H bond, similar to that of the –SH group proposed for the $Zn_4In_2S_7$-based system.
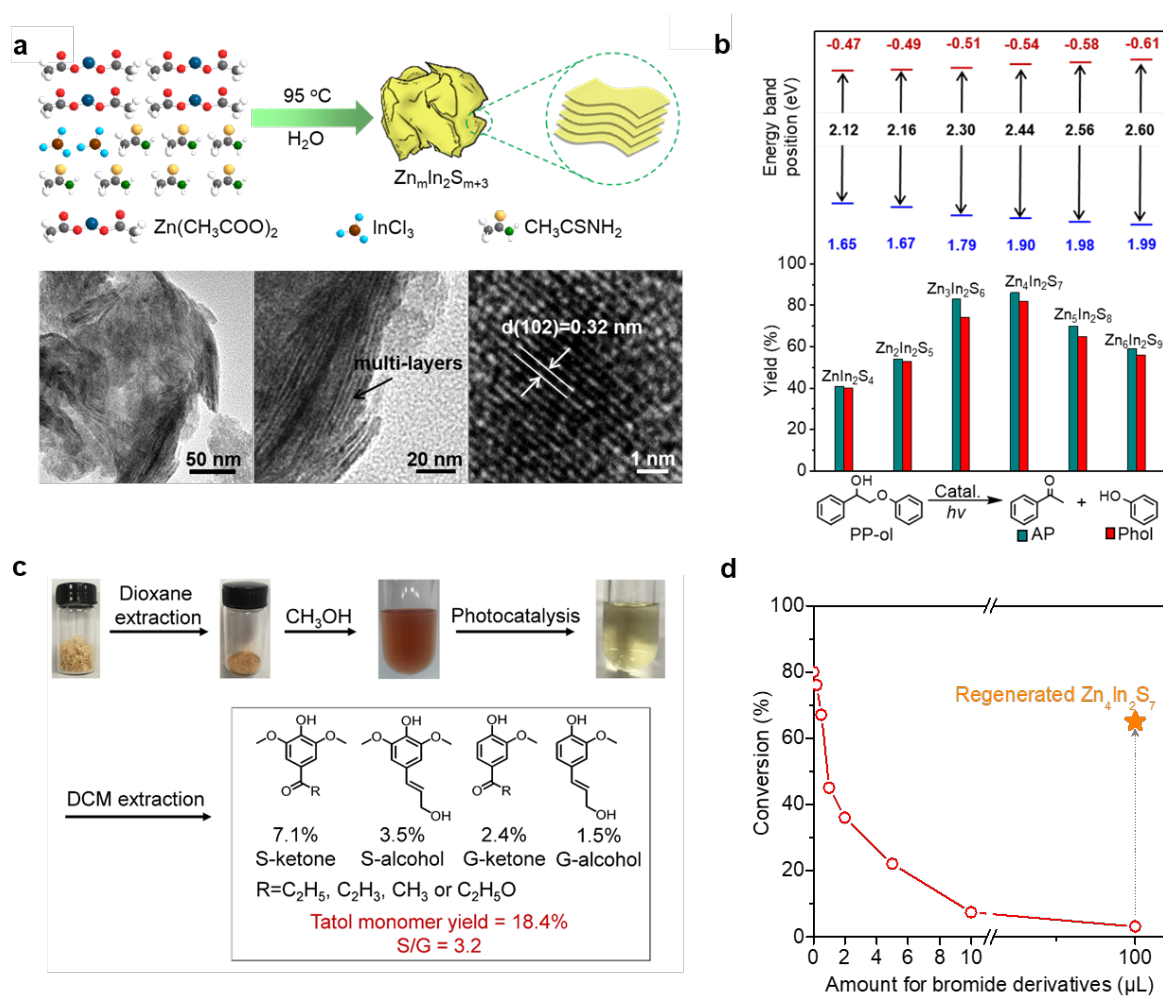
Figure 5. a) Schematic illustration of the synthesis of $Zn_mIn_2S_{m+3}$ (*m*=1-6) samples and TEM, HRTEM images of $Zn_4In_2S_7$. b) Energy-band positions of $Zn_mIn_2S_{m+3}$ (*m*=1-6)

and their photocatalytic activities for the conversion of PP-ol. c) Photocatalytic depolymerization of Organosolv birch lignin over $Zn_4In_2S_7$ under visible-light irradiation. d) Photocatalytic performance of $Zn_4In_2S_7$ after treatment with different amounts of bromide derivatives and the regenerated $Zn_4In_2S_7$. Reproduced with permission.[31] Copyright 2019, Wiley-VCH.

The metal sulfides that can perform one-pot cleavage of β-O-4 linkage include $ZnIn_2S_4$,[51] oxidized Ni/CdS nanosheet,[52] zinc blende CdS,[46] Ag^+-exchanged wurtzite CdS,[55] and $Zn_4In_2S_7$.[31] Different from the two-step method that requires scavengers, these metal sulfide-based one-pot systems are performed in the absence of a sacrificial reagent. Two different mechanisms have been proposed for the β-O-4 bond cleavage over these catalysts, i.e., the self-hydrogenolysis mechanism via C_α=O intermediate and the electron-hole coupled mechanism via C_α radical intermediate (Figure 4). Both mechanisms start with oxidation by photo-generated holes, producing a reaction intermediate with lower C_β−O BDE, followed by participation of photo-generated electrons in the reductive cleavage of C_β−O bond. Surface sulfur atoms are likely responsible for the uniqueness of metal sulfides for the selective cleavage of β-O-4 bond, and this has a biomimetic feature. Glutathione, a thiol redox mediator with nucleophilic and reductive properties, has been found as the key species for the cleavage of lignin β-O-4 bond by S_N2 mechanism in some wood-digesting bacteria such as *Sphingobium* sp. SYK-6.[57, 58] Similar chemical processes using small organic thiols as nucleophilic reagents for the cleavage of the partially oxidized β-O-4 linkages have also been demonstrated.[59, 60] A biomimetic S_N2 C_β−O bond cleavage mechanism involving surface sulfur atoms with localized photogenerated electrons may occur over the metal sulfide catalyst. Further studies on the detailed functions of surface sulfur atoms for the cleavage of β-O-4 bond are needed in the future.

2.2. Conversion of Lignocellulosic Biomass over Quantum Dots

It is worth mentioning that, during the process for extraction of Organosolv lignin from lignocellulosic biomass, the robust C−C cross-linked structures (e.g., β-β' and β-5') would be formed at the expense of more labile β-O-4 linkages.[43] Therefore, the abundance of β-O-4 linkages in Organosolv lignin is lower than that in the native lignin. The direct transformation of native lignin in lignocellulose, which is also known as the lignin-first strategy, can significantly increase the yield of aromatic monomer.[7] Moreover, the lignin-first strategy can avoid the tedious fractionation steps to separate lignin from other fractions in lignocellulosic biomass, since the lignin oil and solid pulp can be easily separated. However, the conversion of native lignin is very challenging. Given native lignin is intertwined with carbohydrates in lignocellulose and is not soluble in almost any organic solvent, the direct contact of solid native lignin with a solid semiconductor photocatalyst is very limited. Therefore, the lignin-first strategy has paid attention to the use of solvents like alcohols or elevated temperatures that can enhance the direct solvolysis and solubilization of the lignin fraction in solution.[61] For photocatalytic conversion of lignocellulose over metal oxide semiconductors under mild conditions, free radicals like OH• usually function as redox mediators, which shuttle the charge carriers from the solid catalyst to the solid substrate. However, these free radical intermediates with strong oxidation potentials normally result in the production of CO_2 as the major carbon-based product. New strategies are needed to improve the intimate contact between the solid catalyst and high MW native lignin structures or lignocellulose.[62, 63]

Recently, Wang and colleagues proposed a "solubilizing" catalyst strategy by using the colloidal nature of QDs to overcome the low efficiency of contact between native lignin and semiconductors.[46] A series of zinc blende CdS QDs (size < 6.4 nm) with mean sizes varying from 3.8 to 6.1 nm were synthesized by a typical hot injection

method. The specific surface area and the redox capability of photogenerated charge carriers for the QDs increased on decreasing their sizes. The photocatalytic activity of CdS QDs for the selective conversion of PP-ol was higher than that of zinc blende CdS NPs. The CdS QDs with a size of 4.4 nm (denoted as CdS QD−4.4 nm) showed the highest product yields, and the rate of PP-ol conversion over CdS QD−4.4 nm was ~4 times higher than that over CdS NPs (Figure 6a).[46]

CdS QD−4.4 nm could efficiently catalyze the conversion of native lignin in birch woodmeal, providing a high yield (27 wt%) of functionalized aromatic monomers. On the other hand, the CdS NPs, which were capable of catalyzing the conversion of lignin model compounds, only showed a very low yield (1.2 wt%) of aromatic monomers in the photocatalytic conversion of native lignin. This demonstrates the effectiveness of the "solubilizing" catalyst strategy in the conversion of *in planta* lignin materials (Figure 6b). This represents the first illustration of photocatalysis in selective depolymerization of native lignin.[46] CdS QDs could also catalyze the depolymerization of different types of technical lignin samples to provide aromatic monomers (1.2%-15%) with near theoretical yields (based on the content of remaining β-O-4 bonds).[64] It is worth mentioning that the yield of aromatics from the conversion of technical lignin samples is significantly lower than that from the conversion of native lignin. Thus, the result confirms that the lignin-first strategy is beneficial to the production of aromatic monomers. Furthermore, the CdS QDs catalyst could be readily separated from the liquid aromatic monomer products and from the remaining solid cellulose/hemicellulose by a reversible aggregation-colloidization strategy.[46] The remaining hemicellulose and cellulose fraction of raw biomass were well preserved and they could further be converted into xylose and glucose by stepwise acidolysis and enzymolysis. Therefore, the photocatalytic lignin-first approach is very promising, not only because high yields of aromatic monomers can be achieved under mild conditions

but also because it can be integrated well with the current biorefinery technology and may assist the accomplishment of full utilization of lignocellulosic biomass.
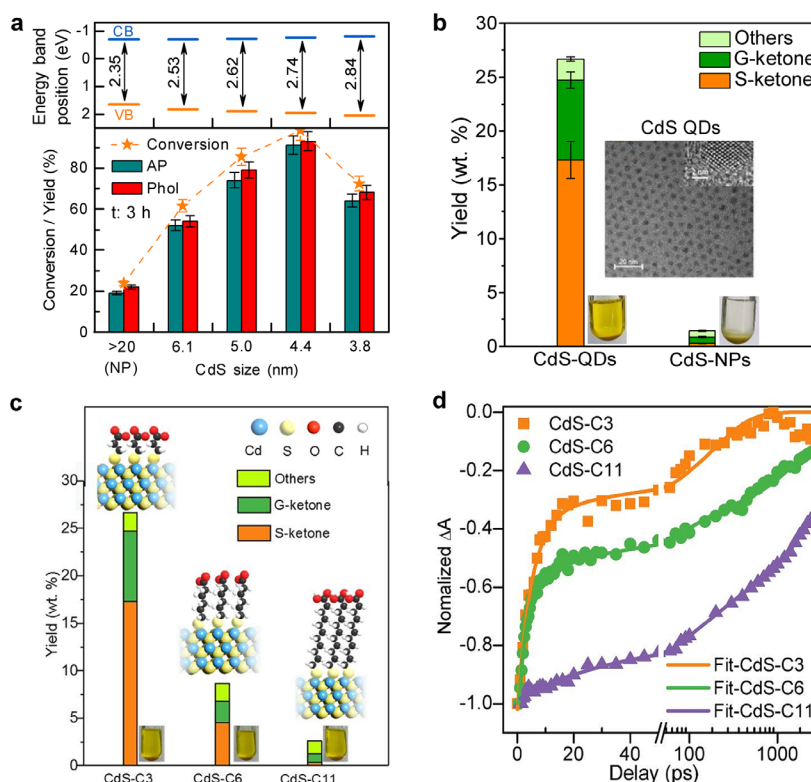
Figure 6. a) Energy-band diagram of CdS with different sizes and their photocatalytic performances in PP-ol conversion. b) Yields of aromatic monomers obtained with CdS QDs and CdS NPs in photocatalytic conversion of native lignin in birch woodmeal. Inset images: TEM of CdS QDs and photos for mixtures of birch woodmeal with CdS QDs and CdS NPs. Reproduced with permission.[46] Copyright 2018, Springer Nature. c) Effect of alkyl chain length of the mercaptoalkanoic acid ligands on CdS QDs (CdS-Cx QDs) on photocatalytic conversion of native lignin. Inset images: schematic illustrations of CdS-Cx QDs and photos for mixtures of birch woodmeal with CdS-Cx QDs. d) Kinetic curves of electron decay in the presence of PP-ol with CdS-Cx QDs. Reproduced with permission.[64] Copyright 2019, American Chemical Society.

It is of interest that the ligands of CdS QDs, which were attached to a large fraction of surface atoms, played an essential role in the conversion of the solid native

lignin. The use of hydrophilic organic ligands for instance resulted in pseudo homogeneous CdS QDs in polar CH_3OH/H_2O solution, allowing intimate contact between QDs and the native lignin, and thus worked efficiently for the depolymerization of native birch lignin.[64] On the contrary, QDs with hydrophobic ligands aggregated in the solvent and led to very limited activity in the conversion of native lignin. In addition, on intentionally decreasing the length of alkyl chains of the hydrophilic mercaptoalkanoic acid ligands, an increase in the catalytic activity for the production of aromatic monomers was observed (Figure 6c).[64] The electron-decay kinetic studies using femtosecond transient absorption spectroscopy for the CdS QDs with different lengths of mercaptoalkanoic acid ligands showed that the rate constant of charge transfer from the QD core to β-O-4 bond decreased exponentially with an increase in the length of mercaptoalkanoic acid ligands (Figure 6d). This result suggests that the charge carriers from the inorganic QD core are transferred to the β-O-4 bond in native lignin through the organic ligand by an electron-tunneling mechanism.[64]

CdS/CdO$_x$ QDs were reported to be efficient catalysts for photo-reforming of native lignocellulosic biomass.[65] The reactions were performed in an alkaline solution with pH above 14, in which *in situ* formation of CdO$_x$ took place on CdS QD surfaces. The formation of a CdO$_x$ shell improved the resistance of CdS QDs to photocorrosion, and thus enhanced the performance for H_2 evolution. The basic conditions also facilitated the dissolution of lignin and polysaccharides into the solution, making the lignocellulose substrate (and its bondings) more available to the photocatalytic process.[65] The CdS/CdO$_x$ QDs in alkaline media exhibited higher efficiencies than a benchmark TiO$_2$|RuO$_2$-Pt catalyst. Further comparative experiments pointed out that the colloidal nature of CdS/CdO$_x$ promoted the interaction with the substrate, and thus enabled the catalyst to show the excellent ability for the reforming of native

lignocellulose at room temperature under visible-light irradiation.[65-67] The system was tolerant to a range of lignocellulosic substrates, including tree branch bagasse, sawdust and grass, as well as wastepaper such as cardboard and newspaper.[66]

OH• radicals are often recognized as the active species for photocatalytic reforming of biomass. However, for the system based on the CdS/CdO$_x$ QD photocatalyst, no OH• could be detected by photoluminescence using terephthalic acid as the OH• trapping reagent, suggesting that OH• was unlikely the dominant active species for the photo-reforming of lignocellulose over CdS/CdO$_x$ QDs.[65] The detected organic products included formate, lactate and acetate as well as C4 and C5 sugars.[66] The product distribution indicated that not only the cleavage of C−O bonds took place, but also more stable C−C bonds in lignocellulose were cleaved over the CdS/CdO$_x$ QD catalyst. The authors proposed that after the partial cleavage of C−O bonds in alkaline solution, lignocellulosic substrates might bind to the CdS/CdO$_x$ QD surface through Cd−O−R bonds. This chemisorption could facilitate hole transfer to the substrate, leading to more efficient oxidation and C−C bond cleavage, which resulted in the coproduction of short-chain organic products with H_2.[65]

3. Upgrading

Lignocellulose-derived chemicals in this section refer to monosaccharides, furanic chemicals and short-chain oxygenates that can be manufactured by the transformation of polysaccharides, as well as aromatics that can potentially be produced by the conversion of lignin. These bio-platforms contain multiple functional groups, which can undergo many possible reaction pathways toward different products. Therefore, selectivity control stands out as one of the most important issues in the transformations of these functionalized bio-platforms.[68, 69] The conversion of aldehyde/hydroxyl groups in polysaccharide-derived platforms, such as 5-hydroxymethylfurfural (HMF) or furfural, can produce bio-based

carbonyl or carboxyl products, which are key intermediates for the production of furanic-based fine chemicals or polymers. Selective oxidation has been one major focus in the research field of selective upgrading of bio-platforms by photocatalysis in the past decade.[4] Photocatalytic coupling of bio-platforms has recently emerged as a new tool for the production of chemicals with large carbon numbers. Lignocellulose-derived short-chain oxygenates can also be converted into valuable products by photocatalytic approaches, such as photocatalytic coupling of ethanol to produce 2,3-butanediol[70] and photocatalytic amination of α-hydroxyl acids to produce alanine[71]. Metal sulfides have been found as efficient catalysts for many selective oxidation, coupling, and amination reactions.

3.1. Selective Oxidation to Produce Carbonyls or Carboxyls

Photocatalytic transformation of bio-platforms was first investigated over metal oxides for H_2 production, in which the bio-platform is considered as a hole scavenger and CO_2 is typically produced as the major product.[72] Strong oxidants like OH• radicals (2.8 V vs SHE)[16] are assumed to be responsible for the mineralization of these organic molecules to CO_2.[73, 74] Selective oxidation of bio-platforms to value-added products rather than CO_2 has received great interest in the past decade.[13, 14, 16] In particular, a great number of efforts have been devoted to the conversion of aldehyde/hydroxyl groups in monosaccharides or monosaccharide-derived platforms (e.g., HMF or furfural) to afford bio-based carbonyl or carboxyl over TiO_2.[4] The key to enhancing the selectivity of these transformations lies in the generation of reactive species such as $O_2\bullet^-$ or photogenerated holes with proper oxidation potential, whereas the formation of highly oxidative species like OH• radicals should be suppressed. Many strategies such as bandgap engineering,[75] co-catalysts modification[76] and addition of external sacrificial reagents[77] have been proposed to improve the selectivity.

As compared to TiO_2, metal sulfides such as CdS have a relatively lower oxidation potentials, and the holes from the VB of CdS are unable to drive the oxidation of OH^- to produce OH• radicals.[78] Therefore, metal sulfides have often been used for selective

oxidation of biomass-derived platform compounds. Photocatalytic oxidation of furfural alcohol and HMF to the corresponding aldehydes or acids with simultaneous evolution of H_2 has been performed over Ni-decorated ultrathin CdS nanosheets (Figure 7).[79] A method of microwave treatment followed by chemical reduction was developed to synthesize 1.1 nm ultrathin CdS wurtzite nanosheets loaded with controllable amounts of Ni without aggregation and segregation; Ni, Cd and S were evenly distributed within Ni/CdS. No formation of OH• radicals was observed during the photocatalytic process as evidenced by photoluminescence and ^{1}H NMR spectroscopy using terephthalic acid as the OH• radical trapping reagent.[79]

Near 100% selectivity for the oxidation of furfural alcohol to furfural and HMF to 2,5-diformylfuran (DFF) was observed over Ni/CdS nanosheets under visible-light irradiation in water solvent. However, the conversion rate of HMF to DFF was only one fifth as compared to that of furfural alcohol to furfural. The control experiments with substituted furfurals as substrates suggested that the presence of an aldehyde group caused the slower oxidation of the alcohol group in HMF. The DFT calculations suggested that the adsorption of HMF via its aldehyde group is 0.13 eV more favorable than that via the alcohol group, indicating that HMF was preferably adsorbed via the aldehyde group on the surface. This would keep the alcohol away from the surface, rendering the oxidation of the alcohol group (in presence of aldehyde) more difficult.[79] It is noteworthy that the pH of the system plays a curial role in controlling the product selectivity. When the solvent was changed from pure water to alkaline solution, the major products obtained from photocatalytic conversions of furfural and HMF were furoic acid and FDCA, respectively (Figure 7), and the product yield could exceed 90% in both cases. The high selectivity of carboxyl products in alkaline may be explained by the involvement of the Canizzaro mechanism. In other words, aldehydes are not stable at high pH and undergo disproportionation into alcohols and carboxylates.[79]
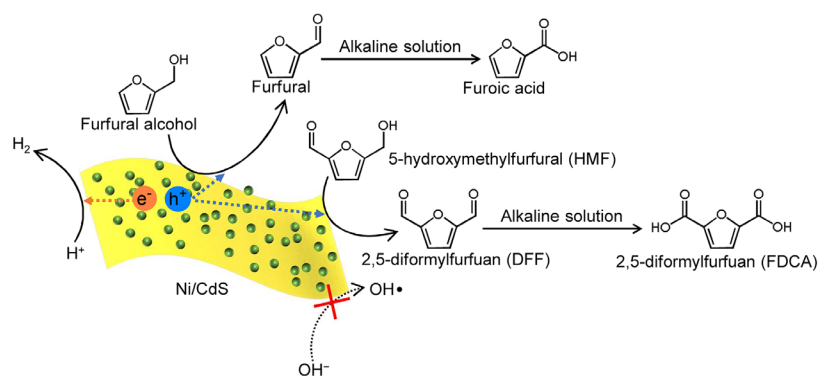
Figure 7. Schematic illustration for photocatalytic oxidative conversions of furfural alcohol and 5-hydroxymethylfurufural over a Ni/CdS nanosheet catalyst.[79]

Phosphorus-doped $Zn_xCd_{1-x}S$ ($Zn_xCd_{1-x}S$-P) semiconductors with rich S vacancies were found as efficient photocatalysts for selective oxidation of HMF to DFF. The photogenerated electrons were used for H_2 evolution.[80] No H_2 was produced over $Zn_xCd_{1-x}S$ ($0 \leq x \leq 1$) catalysts under visible-light irradiation, whereas the evolution of H_2 was observed over the $Zn_xCd_{1-x}S$-P catalysts and the rate of H_2 evolution during water splitting ranged from 30 to > 400 μmol h^{-1} g^{-1}. The $Zn_{0.5}Cd_{0.5}S$-P catalyst exhibited the highest H_2 evolution rate (419 μmol h^{-1} g^{-1}) in pure water. The addition of HMF could enhance the rate of H_2 evolution to 786 μmol h^{-1} g^{-1}, and meanwhile HMF was mainly converted to DFF. After 8 h of photocatalytic reaction, the conversion of HMF was about 40% and the selectivity of DFF was 65%. The interstitial P doping likely promoted the VB position level and the Fermi level of the catalyst. This could prolong the lifetime of charge carriers and enhance the generation and separation of photogenerated electron-hole pairs, resulting in a higher photocatalytic performance.[80]

Efficient photocatalytic transformations of furfural alcohol into furfural coupled with the evolution of H_2 at a high rate have been realized over a $Ti_3C_2T_x$/CdS composite. T in $Ti_3C_2T_x$ represents surface terminations, which could be OH, F or O. $Ti_3C_2T_x$ is one member of a new family of two-dimensional (2D) transition metal carbides, which has drawn recent attention due to their strong light-absorbing ability, inherent electrical conductivity, and lamellar 2D

structure.[81] By using a facile low-temperature wet-chemistry process, the Ti$_3$C$_2$T$_x$ nanosheets were intimately integrated with the CdS matrix. The photocatalytic activity for the selective oxidation over the constructed Ti$_3$C$_2$T$_x$/CdS composite was about 3 times higher compared to that over CdS. A series of photoelectrochemical and photoluminescence (PL) measurements showed that Ti$_3$C$_2$T$_x$ could efficiently extract electrons generated from CdS, thereby facilitating the separation and transport of photoexcited charge carriers. This results in the enhanced photocatalytic performance of the Ti$_3$C$_2$T$_x$/CdS composites.[81]

3.2. Coupling to Produce Large-Carbon-Number Chemicals

Recently, photocatalysis has been applied to the coupling of lignocellulose-derived methylfurans to produce C$_{10}$−C$_{18}$ high-quality diesel fuel precursors over Ru-doped ZnIn$_2$S$_4$ under visible-light irradiation.[82] In Ru-doped ZnIn$_2$S$_4$, Ru atoms were isolated entities incorporated within the ZnIn$_2$S$_4$ lattice by replacing indium ions, and therefore Ru could be considered as a substitutional ion in the Ru-doped ZnIn$_2$S$_4$ material (Figure 8a). The doping of Ru increased the apparent quantum yield (AQY) of ZnIn$_2$S$_4$ from 8.0% to 15.2%. A higher charge separation efficiency of Ru-doped ZnIn$_2$S$_4$ was evidenced by a contact potential difference (CPD$_{light}$–CPD$_{dark}$) analysis (Figure 8b) and photoluminescence. In addition, transient absorption kinetics (Figure 8c) indicated that the lifetimes of charge carriers were prolonged by the Ru doping.[82] The higher charge separation efficiency and longer lifetime of charge carrier of Ru-doped ZnIn$_2$S$_4$ were probably caused by the structural defect induced by doping Ru. With the holes trapped at defect sites, the electron-hole recombination became slower, and thus this may improve the charge-carrier separation efficiency, ultimately providing better catalytic activity.

After light irradiation for 12 h, products from dehydrocoupling of 2,5-dimethylfuran included dimers (4.69 g g$_{catalyst}^{-1}$), trimers (1.84 g g$_{catalyst}^{-1}$), tetramers (0.24 g g$_{catalyst}^{-1}$) and a negligible amount of higher oligomers. Time-course studies showed an increased selectivity of trimers and tetramers with an increase in reaction time, suggesting that trimers and

tetramers might be formed from dimers in a consecutive pathway. Higher oligomers were less inclined to be formed because of the steric hindrance for additional C−C coupling. Radical-trapping experiments revealed that photogenerated holes selectively activated the C_α−H bond in methylfurans, generating furfural radicals as reaction intermediates. Furfural radical intermediates underwent radical resonance and C−C coupling to produce straight-chain dimers, branched-chain dimers, and branched-chain trimers as major products (Figure 8d). H_2 was produced in high efficiency by consuming photogenerated electrons.[82] The activity of the Ru-doped $ZnIn_2S_4$ catalyst decreased slightly during the first 2 h of irradiation, but then remained unchanged afterwards. Operando XANES/EXAFS studies revealed that a part of Ru ions was transformed into Ru clusters or Ru metal NPs during the initial 2 h of irradiation (Figure 8e, 8f), and the content of substitutional Ru ions remained constant after the initial 2 h. The consistence in the decreased catalytic performance and the reduction of the content of substitutional Ru with time suggests that the Ru ions hosted in the $ZnIn_2S_4$ matrix directly participate in the photocatalytic dehydrocoupling reactions, but more evidence is required to corroborate this hypothesis.[82]
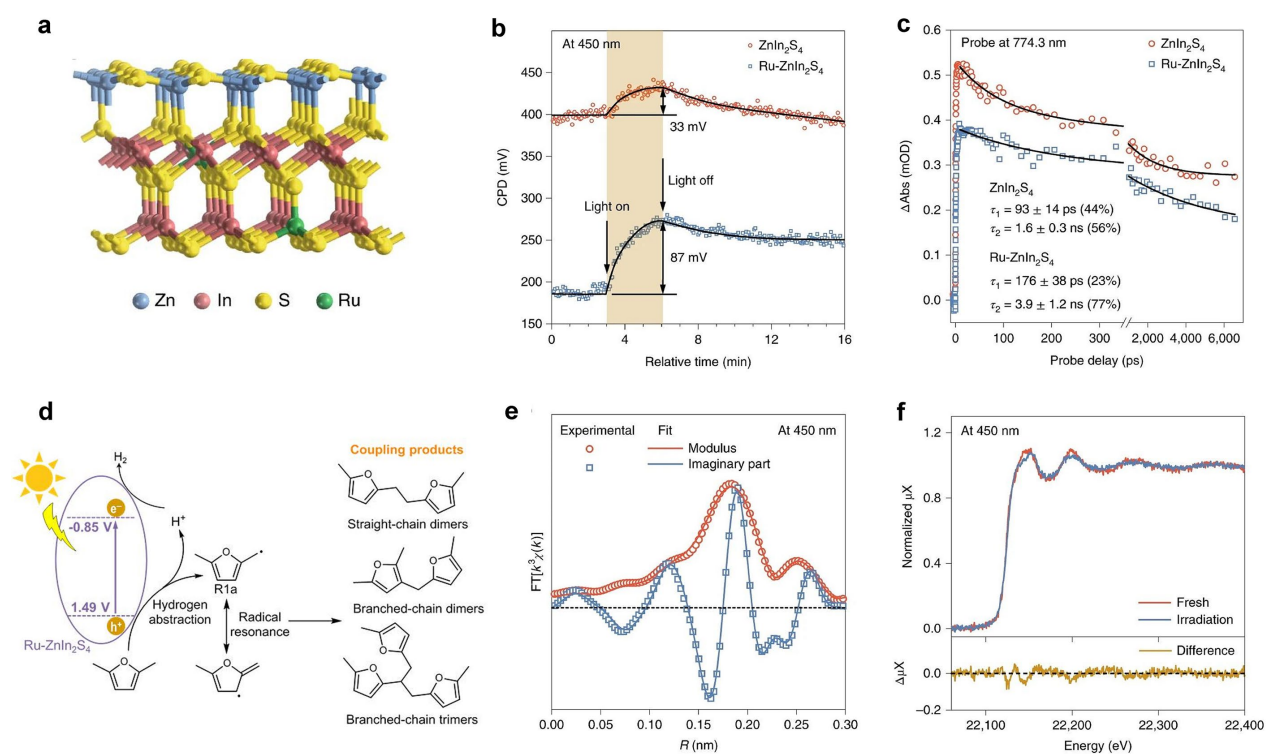
Figure 8. a) Schematic illustration of the Ru-ZnIn2S4 structure. b) Contact potential difference (CPD) of ZnIn2S4 and Ru-ZnIn2S4. c) Transient absorption kinetics of ZnIn2S4 and Ru-ZnIn2S4. d) Proposed mechanism for photocatalytic coupling of methylfurans over Ru-ZnIn2S4 under visible-light irradiation. e) Fit of the FT k^3-weighted $\chi(k)$ of the EXAFS signals of Ru-ZnIn2S4 at the Ru K edge. f) Operando XANES spectra of Ru-ZnIn2S4 at the Ru K edge. Reproduced with permission.[82] Copyright 2019, Springer Nature.

It is noteworthy that the synthesis of coupling products from bio-platforms is very challenging using conventional thermocatalysis, which usually requires homogenous acid catalysts or harsh reaction conditions to achieve such product formation.[83] Therefore, photocatalysis is a promising tool in chain-extension of biomass-derived chemicals under mild conditions because the radical intermediates for C−C coupling reactions can be readily produced by the photogenerated electrons or holes. Homogenous photocatalysts like Ir polypyridyl complex have been used to construct new C−C or C−N bonds from aromatic ketones that can potentially be derived from lignin. However, sacrificial agents such as tertiary amine are usually required in these systems.[4]

Aromatic ketones or aldehydes produced from catalytic depolymerization of lignin can be easily transformed into the corresponding alcohols, which can also undergo a photocatalytic C−C coupling reaction to generate C14+ products. McClelland and Weiss reported that photocatalytic conversion of benzyl alcohol over CdS QDs afforded 36% benzaldehyde and 64% coupling products, i.e., 49% hydrobenzoin (HB) + 7% benzil (BZL) + 8% deoxybenzoin (DOB) (Figure 9a).[84] CdS QDs could catalyze the oxidation of C$_{\alpha}$−H bond in benzyl alcohol to produce benzyl radical, which then underwent further oxidation to benzaldehyde or coupling reactions. Time-course analyses and optical spectra of CdS QDs revealed that the surface Cd^{2+} on CdS QDs was partially reduced into Cd^0 *in situ*, which may

facilitate the reduction of benzaldehyde back to benzyl radical and further to the C−C coupling product (Figure 9b). By addition of electron scavenger, such as anthroquinone-2-sulfonate, to intentionally suppress the reduction of surface Cd^{2+} to Cd^0, benzaldehyde was formed with 99% selectivity. This result underscores the important role of *in situ* photo-deposited Cd^0 in enhancing the selectivity toward coupling products. Given these results, the authors further added $Cd(ClO_4)_2$ to the reaction mixture to increase the number of surface Cd^0, and after optimizing the reaction conditions, a high selectivity of 91% toward coupling products (68% HB + 15% BZL + 8% DOB) was achieved (Figure 9a).[84]

It is worth mentioning that the manufacture of DOB, an important precursor with versatile applications, requires the consumption of a stoichiometric amount of toxic PCl_3 or $SOCl_2$ in the current chemical industry. Photocatalytic coupling of benzyl alcohol can offer DOB with a high yield and can avoid the use of expensive and environmental harmful reagents, and thus is a highly desirable alternative. A recent study has succeeded in controlling the selectivity of coupling products during the photocatalytic oxidation of benzyl alcohol by changing the Zn/In ratio in Zn-In-S semiconductors. For instance, an increase in the ratio of Zn/In from 0.05 to 0.4 resulted in an increase in the yield of DOB from 24% to 59% at the expense of the yield of benzoin (BZ), which decreased from 65% to 8%.[85] Mechanistic studies showed that the reaction intermediate was HB (Figure 9c), which was generated by the activation of the C_α−H bond in benzyl alcohol to benzyl radical over Zn-In-S, followed by the direct coupling of benzyl radical. The conversions of HB to DOB and BZ were both initiated by C−H bond activation through the acceptance of photo-generated holes from Zn-In-S. The radical intermediate could undergo either further oxidation to produce BZ or reductive cleavage of the C−OH bond to produce DOB. A sufficient reduction potential is required to drive the cleavage of the C−OH bond for the formation of DOB. Such a high reduction ability of Zn-In-S could be gained by increasing the Zn/In ratio. For instance, the conduction-band potential decreased from –2.68 V for $Zn_{0.2}In_2S_{3.2}$ to –2.85 V for $Zn_{0.6}In_2S_{3.6}$.

Therefore, the Zn-In-S catalyst with a higher Zn/In ratio showed higher C−OH bond cleavage ability, leading to higher DOB selectivity (Figure 9c).[85]

Sun and co-workers also reported that a two-dimensional $ZnIn_2S_4$ could catalyze the oxidative coupling of benzyl alcohol to produce DOB and BZ as major products.[86] A series of control experiments with different substrates and scavengers revealed that the back reduction of benzaldehyde to benzyl radical by photogenerated electrons over $ZnIn_2S_4$ was a critical step for the C−C coupling reaction. The deposition of metallic Ni on $ZnIn_2S_4$ could abstract the electrons for H_2 evolution and inhibit the back reduction of benzaldehyde to benzyl radical. Such deposition resulted in 90% benzaldehyde yield. It was proposed that an acidic environment favored the dehydration reaction to DOB; by further addition of 1 equiv. acetic acid into the reaction mixture, a high yield (73%) of DOB was gained. On the contrary, the addition of water could inhibit the dehydration, resulting in BZ with 83% yield. Besides, $ZnIn_2S_4$ was also able to catalyze homo-coupling of furfural in the presence of an electron scavenger and the hetero-coupling of furfural with furfural alcohol, both resulting in hydrofuroin with yields of > 90% (Figure 9d).[86]
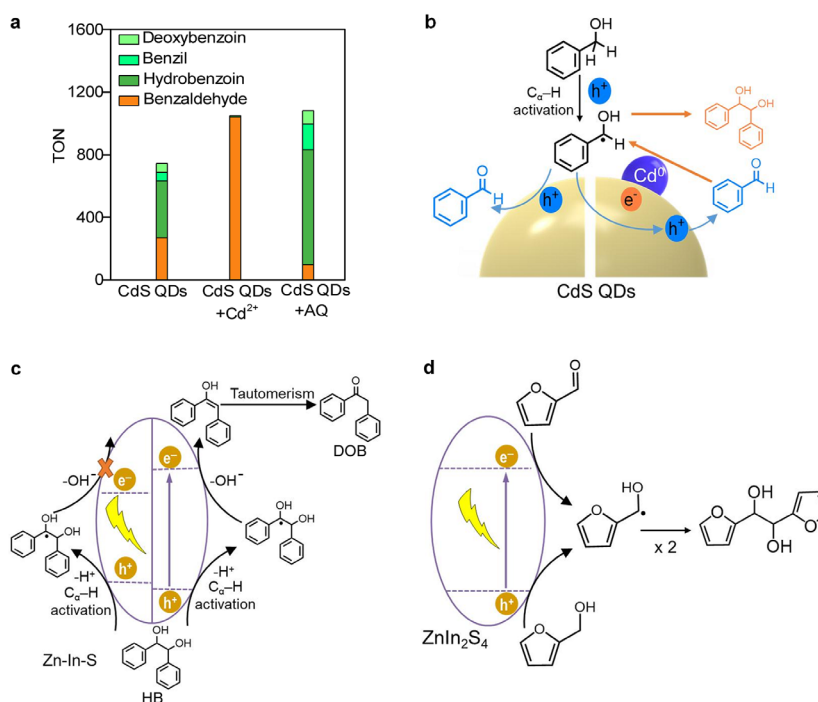
Figure 9. a) Transformations of benzyl alcohol over CdS QDs in the absence and presence of different additives. b) Schematic illustration of different reaction pathways over CdS QDs with or without Cd^0 deposits. Adapted from McClelland et al.[84] Copyright 2019, American Chemical Society. c) Schematic illustration of the proposed mechanism for controllable production of coupling products by tuning the Zn/In ratio in Zn-In-S.[85] d) Proposed reaction pathways for photocatalytic production of hydrofuroin from cross-coupling of furfural and furfural alcohol over $ZnIn_2S_4$.[86]

3.3. Selective Transformation of Short-Chain Oxygenates to Produce Diols and Amino Acids

Ethanol is a primary biorefinery building block that can be derived from biomass and has been identified as a key bio-platform molecule for chemical production.[69, 87] Methanol, which is traditionally produced from natural gas, coal and biomass via syngas, can also be produced from biomass-derived polyols and sugars directly,[88] holding potential as a bio-platform chemical. Both C_2H_5OH and CH_3OH can be converted to diols, such as 2,3-butanediol (2,3-BD) and ethylene glycol (EG), through photocatalytic preferential activation of C−H bond and C−C coupling.[70, 89, 90] 2,3-BD and EG are important chemicals that are used as antifreeze, fuel additives, and in particular as monomers for the production of polymers such as poly(ethylene terephthalate), i.e., PET.

Recently, Wang and co-workers synthesized a series of visible-light-responsive few-layer $Zn_mIn_2S_{m+3}$ ($m = 1−3$) semiconductors with a tunable bandgap energy (E_g) for the conversion of C_2H_5OH under visible-light irradiation (Figure 10a,b).[70] $Zn_2In_2S_5$ and $Zn_3In_2S_6$ displayed selectivities higher than 40% towards the formation of 2,3-BD, while $ZnIn_2S_4$ only provided CH_3CHO (Figure 10c).The modification of $Zn_2In_2S_5$ with cobalt phosphide (CoP) co-catalyst facilitated the charge separation and promoted its photocatalytic performance, showing 53% 2,3-BD selectivity at a H_2 formation rate of 8.5 mmol $g^{-1} h^{-1}$. In contrast to the

UV-light responsive TiO_2 catalyst,[90] the $CoP/Zn_2In_2S_5$ catalyst represents the first example of photocatalyst that is able to produce 2,3-BD from C_2H_5OH driven by visible light, which enables a better use of solar energy.
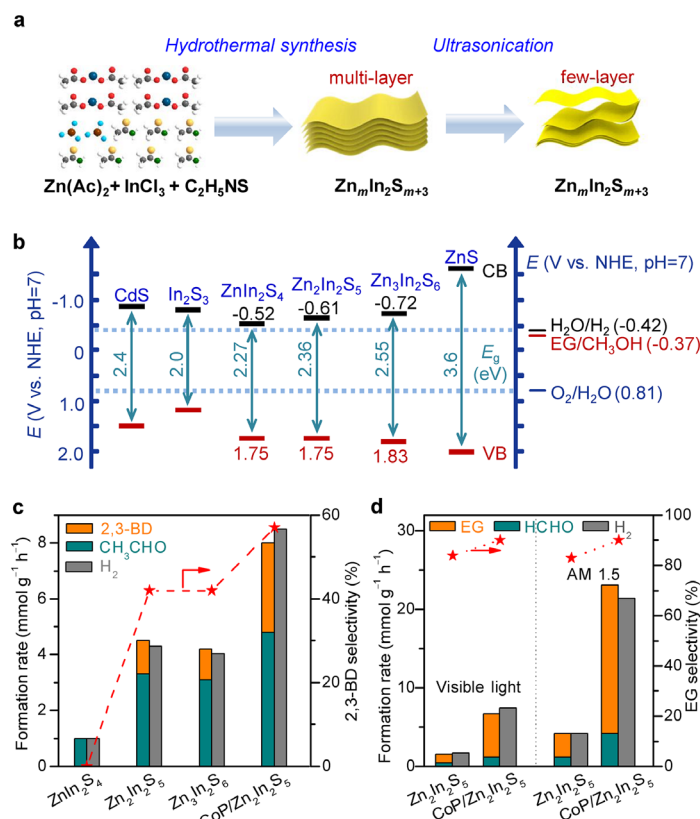
Figure 10. a) Schematic illustration of the synthesis of $Zn_mIn_2S_{m+3}$ semiconductors. b) Energy levels of several related redox couples and band-edge positions of some semiconductors. c) Photocatalytic performances for the coupling of C_2H_5OH to 2,3-BD under visible-light irradiation. d) Photocatalytic performances for the coupling of CH_3OH to EG under visible-light and AM 1.5-light irradiation. Reproduced with permission.[70] Copyright 2020, Royal Society of Chemistry.

Wang and co-workers also reported the first visible-light-driven dehydrogenative coupling of CH_3OH into EG over CdS-based photocatalysts.[89] Among the series of typical photocatalysts for CH_3OH conversion, TiO_2, ZnO, Cu_2O, g-C_3N_4, Bi_2S_3 and CuS provided HCHO as the major product, whereas ZnS and CdS were found to be unique photocatalysts

for the C−C coupling of CH3OH to EG (Figure 11a). The selectivity and formation rate of EG over CdS nanorods were 71% and 0.46 mmol g^{-1} h^{-1}, respectively. HCHO was a major by-product along with EG and H2. The ratio of photogenerated electrons and holes consumed in the product formation was estimated by assuming Equations 1-3, and the value for CdS was close to 1.0. This result confirms the occurrence of reactions of Equations 1-3 for EG, HCHO and H2 formations.

$$2CH_3OH + 2h^+ \rightarrow HOCH_2CH_2OH + 2H^+ \qquad (1)$$

$$CH_3OH + 2h^+ \rightarrow HCHO + 2H^+ \qquad (2)$$

$$2H^+ + 2e^- \rightarrow H_2 \qquad (3)$$
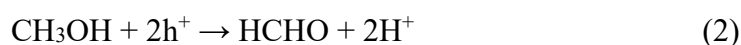
CdS nanorods exhibit better performance for EG formation when compared to other CdS catalysts having different morphologies.[89] Among some typical co-catalysts (Pt, Pd, NiO$_x$, and MoS2) loaded onto CdS nanorods, MoS2 showed the best performance for EG formation; not only the formation rate of EG was increased but also the selectivity of EG was significantly enhanced by the addition of MoS2.[89] MoS2 nanofoams had a better performance for EG formation than MoS2 nanosheets. The formation rate and selectivity of EG were 6.0 mmol g^{-1} h^{-1} and 84%, respectively, over MoS2-sheet/CdS-rod, while they reached 11 mmol g^{-1} h^{-1} and 90% over MoS2-foam/CdS-rod (Figure 11b). The rate of EG formation over the MoS2-foam/CdS-rod catalyst was about 24 times higher than that over the unmodified CdS nanorods. The higher activity of MoS2-foam/CdS-rod was explained by the higher content of edge sites in MoS2 nanofoams and the more intimate contact between MoS2 foams and CdS nanorods (Figure 11c). Thus, the H2 evolution was facilitated over the MoS2 foam co-catalyst, and meanwhile the separation of photogenerated electron-hole pairs was accelerated, favoring the oxidative coupling of methanol to EG (Figure 11d). By designing a process-intensified reactor with EG separation ability, the 90% EG selectivity could be kept during 100 h of reaction, offering an EG yield of 16% over the MoS2-foam/CdS-rod catalyst. A CoP/Zn2In2S5 photocatalyst also demonstrated high efficiencies for the oxidative coupling of CH3OH to EG,

and EG selectivity of 90% and formation rate of 18.9 mmol g^{-1} h^{-1} could be achieved under irradiation by the simulated sunlight (AM1.5) (Figure 10d).

Mechanistic studies revealed that the α-C−H bond of C_2H_5OH could be selectively activated by photogenerated holes over $Zn_2In_2S_5$, resulting in the formation of α-hydroxyethyl radical (•CH(OH)CH$_3$), which then coupled to produce 2,3-BD.[70] Similarly, EG was formed via C−C coupling of hydroxymethyl radical (•CH$_2$OH) from methanol over $Zn_2In_2S_5$ and CdS catalysts.[70, 89] The DFT calculations unravel that, on TiO_2 surfaces, CH_3OH has strong adsorption energy (−1.4 eV) and the OH group has moderate deprotonation energy. Here, the deprotonation energy refers to the energy change for the deprotonation of adsorbed methanol on TiO_2 (110) surface. The O−H bond is easily activated through proton transfer (PT) to CH_3O^- and then to $CH_3O•$ via electron transfer (ET). The formed $CH_3O•$ radical further undergoes oxidation to HCHO as the product (Figure 11e).[89] In contrast, CH_3OH has a negligible adsorption energy (−0.1 eV) on CdS surfaces and is difficult to deprotonate. This enables the preferential activation of the α-C−H bond instead of the O−H bond. The selective cleavage of C−H bond in CH_3OH on CdS to produce •CH$_2$OH occurs through a concerted proton-electron transfer (CPET) mechanism with a low activation barrier (0.8 eV) (Figure 11e). The formed •CH$_2$OH intermediate has a low adsorption energy (−0.2 eV), enabling fast desorption from CdS surfaces to undergo subsequent C−C coupling to EG.
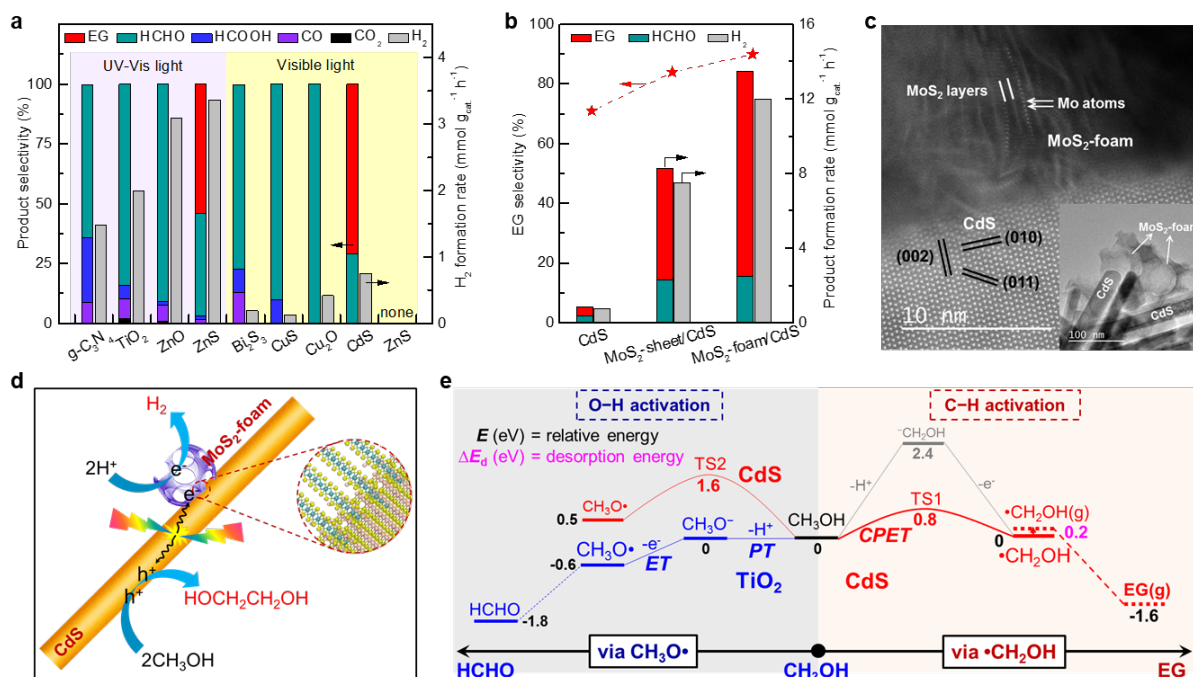
Figure 11. a) Catalytic performances of some typical semiconductors for CH₃OH conversion. b) Catalytic performances of MoS₂-sheet/CdS and MoS₂-foam/CdS-rod. c) High-resolution HAADF-STEM image of MoS₂-foam/CdS-rod (inset: HRTEM). d) Schematic illustration of MoS₂-foam/CdS-rod for the photocatalytic synthesis of EG and H₂ from CH₃OH. e) Reaction energy profiles via •CH₂OH and CH₃O• on CdS (100) and rutile TiO₂ (110). Reproduced with permission.[89] Copyright 2018, Springer Nature.

As compared to the photo-oxidative coupling of bio-platforms, the studies on photo-reductive coupling are relatively limited. Recently, Wang and co-workers have successfully controlled the reaction pathways between photocatalytic hydrogenation and reductive C−C coupling for lignocellulose-derived platform chemicals including furfural, methyl furfural, and vanillin.[91] It is discovered that the product selectivity depends strongly on catalyst morphology and thus on the exposed facet of TiO₂ photocatalyst. Further mechanistic studies revealed that the *in-situ* generated surface oxygen vacancies, which were formed upon irradiation under UV light in methanol solvent, played a decisive role in the selectivity control. The density of oxygen vacancies governed the charge distribution and adsorption strength of

surface species, and thus controlled the product selectivity. For the surfaces without oxygen vacancies, the interaction between reactants and the surface was quite weak. The higher electronegativity of oxygen atom as compared to carbon in the carbonyl group would render the O atom negatively charged, and thus it could be hydrogenated more favorably, leading to the preferential formation of the •C−OH intermediate. This •C−OH intermediate only has weak adsorption characteristics on the surface, enabling facile desorption, followed by C−C coupling.[91] Although the photocatalyst used here is TiO_2 instead of metal sulfides, it is useful to emphasize that the weak interaction of the surface with the reactant is essential to the coupling chemistry for the biomass-derived chemicals, similar to the systems for the oxidative coupling of ethanol and methanol over metal sulfide semiconductors.

Recently, Yan and co-workers found that CdS could efficiently catalyze the amination of a broad range of biomass-derived short-chain α-hydroxyl acids into amino acids using NH_3 as an amination reagent at 50 °C under visible-light irradiation.[71] They observed a morphology-dependent performance of CdS for the photo-amination of lactic acid to alanine. Ultrathin CdS nanosheets displayed the best catalytic performance; the formation rate of alanine over the ultrathin CdS nanosheets was about five times higher than those over the commercial CdS, CdS nanospheres and CdS nanorods, and 35 times higher than that of CdS nanowires. In-depth studies show that both electrons and holes were involved in the reaction. The holes generated on CdS transforms lactic acid into pyruvic acid, which reacts with NH_3 to give an imine. Imine then accepts protons and electrons, leading to alanine. It is of interest that CdS catalysts with all morphologies provided a similar amination rate when pyruvic acid was used as the substrate, indicating that the rate-determining step was the oxidation of lactic to pyruvic acid.[71]

A series of control experiments, kinetic studies and DFT calculations further reveal that the abstraction of the C_α−H from lactic acid in the initial dehydrogenation is the overall rate-determining step. The higher performance of CdS nanosheets in the animation process is

mainly attributed to the higher activity in the kinetically slow C_α−H abstraction step and the poorer activity in the competitive H_2 evolution reaction. This photocatalytic amination system could be applied well to the transformations of several biomass-derived hydroxyl acids. A higher reactivity of the substrate with a lower C_α−H bond dissociation energy corroborates the rate-limiting C_α−H abstraction. It is of interest that under alkaline conditions in the presence of CdS nanosheet, glucose could be directly converted into alanine probably via lactic acid intermediate. This may be a promising photochemical alternative to the current sugar-to-amino acid (fermentation) process.

4. Conclusion and Outlook

The transformation of lignocellulosic biomass into carbon-based fuels and chemicals is of great importance in the pursuit of a sustainable future. Photocatalysis has emerged as a new and effective tool for the valorization of lignocellulose under mild conditions. The unique reaction mechanism of photocatalysis enables precise cleavage of C−O and C−C bonds in macromolecular lignocellulosic components and selective transformations of specific functional groups in lignocellulose-derived platforms.[4] The key to the photocatalytic transformation of lignocellulosic biomass is the active and selective photocatalyst. The present article has demonstrated that metal sulfide semiconductors represent a unique group of photocatalysts that are efficient for a broad range of important yet challenging transformations in the field of lignocellulose valorization.

Several metal sulfides, including $ZnIn_2S_4$,[51] oxidized Ni/CdS nanosheet,[52] zinc blende CdS,[46] Ag^+-exchanged wurtzite CdS,[55] and $Zn_4In_2S_7$[31], are highly efficient for the selective cleavage of C_β−O bond in β-O-4 linkage, the most abundant linkage in lignin. In fact, to the best of our knowledge, the heterogeneous photocatalysts that can perform one-pot cleavage of C_β−O bond in the absence of sacrificial reagents are all based on metal sulfides. Two different mechanisms have been proposed for β-O-4

bond cleavage over the metal sulfide catalyst, i.e., the self-hydrogenolysis mechanism via C_α=O intermediate and the electron-hole coupled mechanism via a C_α radical intermediate (Figure 4). Both mechanisms are initiated by oxidation to form intermediates with lower C_β−O BDEs. Interestingly, a similar process can be found in nature; thiols in wood-digesting bacteria with high nucleophilicity are able to drive the C_β−O cleavage in the oxidized β-O-4 motif by S_N2 attack.[57, 58] The sulfide-based photocatalytic system for the C_β−O bond cleavage may represent a functional, if not a formal, biomimetic system of the biological process. Photogenerated electrons migrating to the surface of metal sulfides generate highly nucleophilic species similar to thiols in bacteria. These surface species with high nucleophilicity can facilitate the cleavage of C_β−O in a similar biomimetic S_N2 mechanism. This may be the origin of the unique photocatalytic C_β−O cleavage property of metal sulfides (Figure 12, upper left panel).

Metal sulfide QDs catalyze the direct conversion of native lignin in lignocellulose[46, 64] and raw lignocellulosic biomass[65, 66] without need of fractionation. The colloidal nature of QDs ensures intimate contact with the lignin substrate, and the ligands of QDs mediate the charge transfer between QDs and the targeted β-O-4 bond. The rational design of ligands with proper substrate compatibility and high electron-mediating ability would enhance the performance of QD catalysts in native lignin valorization. Selective transformations of native lignocellulose by photocatalysis is an important challenge with few successes. The QD photocatalyst has opened an avenue for this alluring research direction.

Bio-based carbonyl or carboxyl products can be obtained in high efficiencies by photocatalytic oxidation of lignocellulose-derived platforms with metal sulfide catalysts.[79−81] The mild oxidation power of metal sulfides contributes to the selective oxidation without the generation of too strong oxidants such as the unselective OH•

radical (Figure 12, upper right panel).[78] The easily tunable band structure of metal sulfides can also enable us to tailor the selectivity of the oxidation without compromising the activity.

Photocatalytic coupling has emerged as a useful tool for the upgrading of bio-platforms to produce large-carbon-number products and diols, and metal sulfides are the most efficient catalysts for this chemistry.[70, 82, 84-86, 89] Selectivity control is a very challenging task in this area. The product selectivity for the oxidative photo-coupling over metal sulfides has been successfully controlled by metal deposition,[84, 86] bandgap engineering,[85] and changing reaction conditions[86]. Several studies have demonstrated that the adsorption energies of bio-platforms and radical intermediates on surfaces of metal sulfides (e.g., CdS) play a crucial role in determining the product selectivity; the low values of adsorption energies would favor the desorption of radical intermediates and thus the formation of coupling products (Figure 12, bottom left panel).[89]

Many recent studies have pointed out that metal sulfides can efficiently drive the photocatalytic activation of C_α−H bond in a variety of bio-platforms, such as benzyl alcohol,[84-86] furanic compounds,[82, 86] and short-chain oxygenates,[70, 89] to produce C_α radicals for subsequent reactions, in particular C−C coupling. The ability of metal sulfides to oxidatively activate the C_α−H has also been discovered in the selective cleavage of lignin β-O-4 linkages through the C_α radical intermediates[31, 46, 55, 64] and in the amination of bio-platforms[71]. The unique activity of metal sulfides for the C_α−H activation may be attributed to the presence of thiol-like species on their surfaces.[31] The surface S atom may act as a Lewis-base site, bonding with protons in the solvent and forming thiol-like species (Figure 12, bottom right panel). Similar thiols have been recognized in a broad range of enzymatic processes and are now widely used in synthetic chemistry.[92] By accepting photogenerated holes, the thiol-like species on metal sulfide surfaces may be transformed into corresponding radicals, which are highly reactive in C−H activation

(Figure 12, bottom right panel). In this regard, metal sulfides can be considered as very promising materials for a great number of organic synthesis reactions involving the construction of new C−C and C−N bonds under mild conditions. The current studies for photocatalytic coupling over metal sulfide semiconductors have mainly focused on homo-coupling reactions. Developing new systems for efficient cross-coupling reactions will certainly extend the scope of products and applications. Controlling the reactive radical intermediates to perform cross-coupling instead of homo-coupling reactions is therefore a future challenge for metal sulfide-based photocatalysis.
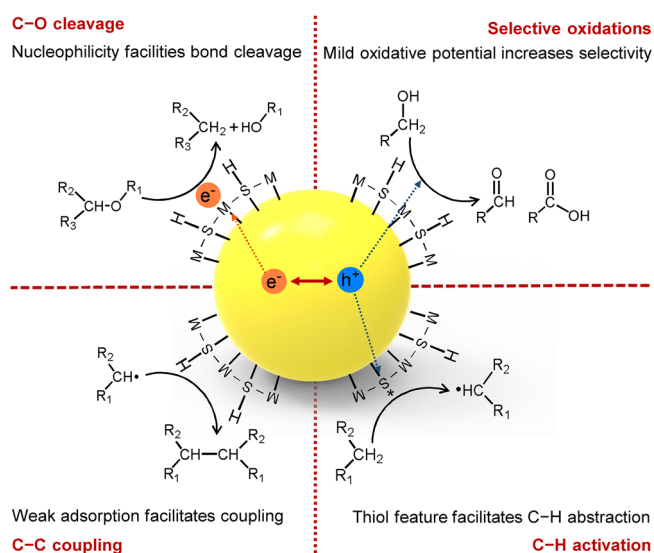
Figure 12. Properties of metal sulfides that may contribute to their unique roles in C−O bond cleavage (upper left panel), selective oxidation (upper right panel), C−C coupling (bottom left panel), and C−H activation (bottom right panel) for photocatalytic biomass valorization.

The field of metal sulfide-based photocatalytic biomass valorization is still in its infancy. CdS is the most investigated metal sulfide photocatalyst, but its practical application is hindered by the intrinsic toxicity of cadmium. The vast variety of metal sulfides encourages future studies to discover more efficient and environmental friendly non-toxic materials. For example, layered transition metal dichalcogenides, such as MoS_2, WS_2, possess the advantages of layered structure, highly exposed active sites and high charge carrier mobility,

and thus may present high efficiencies in photocatalytic lignocellulose valorization.[93] Other emerging photocatalytic materials like I-III-VI$_2$ and I$_2$-II-IV-VI$_4$ semiconductors, which have been proven to be efficient photocatalysts in a range of important reactions such as H$_2$ evolution,[23] may also hold great potentials in biomass valorization.

Oxidative photocorrosion is a common problem faced by metal sulfide photocatalysts.[94] Many metal sulfides performed well for short periods but showed decreased performances over time during lignocellulose transformations. We believe that the photocorrosion may be suppressed by quickly consuming photogenerated holes for biomass conversions. For the reaction, in which the photo-oxidation of chemicals is kinetically slow, the addition of a redox mediator may also increase the long-term durability. Redox mediators such as Fe^{2+}/Fe^{3+} and TEMPO/TEMPO$^+$ may extract photogenerated holes timely to avoid photocorrosion, and then pass the holes to the substrate. The chemical stability of metal sulfides in a wide range of pH is a technical challenge that needs to be addressed. In particular, the production of acidic products (e.g., FDCA and furoic acid) is an important type of biomass valorization, but metal sulfides may be vulnerable under acidic conditions. Thus, the separation of acid products timely with a suitably designed reactor would be beneficial to catalyst stability. An alternative solution is to integrate metal sulfides with protective materials to form a composite photocatalyst that is resistant to photocorrosion under acidic conditions.

In-depth insights into active sites and reaction mechanisms for many related reactions are still less accumulated. Most of the current mechanistic studies focus on organic transformations initiated by photogenerated charge carriers and much effort has been put into tuning the electronic structure of metal sulfides to match the redox potentials or increasing the separation of charge carriers. Few studies have been devoted to elucidating the active sites on metal sulfide surfaces, the functioning mechanism of surface active sites, and the reactions at the photocatalyst-reactant solution interface. The surface- or interface-centered investigation may enable the better control of elementary reactions. Therefore, metal sulfides with defined

and tunable surface structures and properties should be synthesized to build the surface-reactivity relationships. For example, the surface of CdS QDs can be manipulated to be Cd-rich or S-rich,[95] which may help to unravel the active site on CdS surfaces in a specific reaction. Ultrafast spectroscopy and *in situ* characterizations should also be applied to monitor the change of catalyst surfaces during the reaction to offer information on surface adsorbed species and reaction intermediates.

Photocatalysis under mild reaction conditions has emerged as a promising approach for the transformations of lignocellulosic biomass into carbon-based fuels and chemicals. Significant advances have been achieved using metal sulfides as photocatalysts for the valorization of lignocellulosic biomass, including the depolymerization of lignin, the direct conversion of raw lignocellulosic biomass, the selective oxidation, and the coupling and amination of bio-platforms. Metal sulfides in these systems show unique performances in several important and challenging elementary chemical reactions such as C−O cleavage, selective oxidation, C−C coupling, and C−H activation. With these exceptional catalytic activities and selectivities, metal sulfides will continue to play a key role in the field of photocatalysis and green chemistry. We believe that this Progress Report can inspire many future studies on metal sulfide-based photocatalytic systems en route to a sustainable chemical society.

Conflict of Interest

The authors declare no conflict of interest.

References

[1]   J. B. Zimmerman, P. T. Anastas, H. C. Erythropel, W. Leitner, *Science* **2020**, *367*, 397.

[2]   P. Lanzafame, G. Centi, S. Perathoner, *Chem. Soc. Rev.* **2014**, *43*, 7562.

[3]   N. S. Lewis, *Energy Environ. Sci.* **2016**, *9*, 2172.

[4]   X. Wu, N. Luo, S. Xie, H. Zhang, Q. Zhang, F. Wang, Y. Wang, *Chem. Soc. Rev.* **2020**, *49*, 6198.

[5]   C.-H. Zhou, X. Xia, C.-X. Lin, D.-S. Tong, J. Beltramini, *Chem. Soc. Rev.* **2011**, *40*, 5588.

[6]   Z. Zhang, J. Song, B. Han, *Chem. Rev.* **2017**, *117*, 6834.

[7]   W. Schutyser, T. Renders, S. Van den Bosch, S. F. Koelewijn, G. T. Beckham, B. F. Sels, *Chem. Soc. Rev.* **2018**, *47*, 852.

[8]   Z. Sun, B. Fridrich, A. de Santi, S. Elangovan, K. Barta, *Chem. Rev.* **2018**, *118*, 614.

[9]   D. M. Schultz, T. P. Yoon, *Science* **2014**, *343*, 1239176.

[10]   T. P. Yoon, M. A. Ischay, J. Du, *Nat. Chem.* **2010**, *2*, 527.

[11]   H. Huo, X. Shen, C. Wang, L. Zhang, P. Rose, L.-A. Chen, K. Harms, M. Marsch, G. Hilt, E. Meggers, *Nature* **2014**, *515*, 100.

[12]   D. G. Nocera, *Acc. Chem. Res.* **2017**, *50*, 616.

[13]   X. Liu, X. Duan, W. Wei, S. Wang, B.-J. Ni, *Green Chem.* **2019**, *21*, 4266.

[14]   L. I. Granone, F. Sieland, N. Zheng, R. Dillert, D. W. Bahnemann, *Green Chem.* **2018**, *20*, 1169.

[15]   S.-H. Li, S. Liu, J. C. Colmenares, Y.-J. Xu, *Green Chem.* **2016**, *18*, 594.

[16]   J. C. Colmenares, R. Luque, *Chem. Soc. Rev.* **2014**, *43*, 765.

[17]   J. C. Colmenares, R. S. Varma, V. Nair, *Chem. Soc. Rev.* **2017**, *46*, 6675.

[18]   J. C. Colmenares, *Curr. Opin. Green Sustain. Chem.* **2019**, *15*, 38.

[19]   J. Xuan, W.-J. Xiao, *Angew. Chem. Int. Ed.* **2012**, *51*, 6828.

[20]   Y. Wang, Y. Liu, J. He, Y. Zhang, *Sci. Bull.* **2019**, *64*, 1658.

[21]   P. Sudarsanam, R. Zhong, S. Van den Bosch, S. M. Coman, V. I. Parvulescu, B. F. Sels, *Chem. Soc. Rev.* **2018**, *47*, 8349.

[22]   M. Yasuda, T. Matsumoto, T. Yamashita, *Renew. Sustain. Energ. Rev.* **2018**, *81*, 1627.

[23]   M. D. Regulacio, M.-Y. Han, *Acc. Chem. Res.* **2016**, *49*, 511.

[24]   L. Cheng, Q. Xiang, Y. Liao, H. Zhang, *Energy Environ. Sci.* **2018**, *11*, 1362.

[25]   K. Zhang, L. Guo, *Catal. Sci. Technol.* **2013**, *3*, 1672.

[26]   Y. Xu, M. A. A. Schoonen, *Am. Mineral.* **2000**, *85*, 543.

[27]   B. Ao, *Acta Mater.* **2020**, *186*, 597.

[28]   R. Woods-Robinson, Y. Han, H. Zhang, T. Ablekim, I. Khan, K. A. Persson, A. Zakutayev, *Chem. Rev.* **2020**, *120*, 4007.

[29]   K. J. Chang, S. Froyen, M. L. Cohen, *Phys. Rev. B* **1983**, *28*, 4736.

[30]   S. Chandrasekaran, L. Yao, L. Deng, C. Bowen, Y. Zhang, S. Chen, Z. Lin, F. Peng, P. Zhang, *Chem. Soc. Rev.* **2019**, *48*, 4178.

[31]   J. Lin, X. Wu, S. Xie, L. Chen, Q. Zhang, W. Deng, Y. Wang, *ChemSusChem* **2019**, *12*, 5023.

[32]   G. Hautier, A. Miglio, G. Ceder, G.-M. Rignanese, X. Gonze, *Nat. Commun.* **2013**, *4*, 2292.

[33]   H.-L. Wu, X.-B. Li, C.-H. Tung, L.-Z. Wu, *Adv. Mater.* **2019**, *31*, 1900709.

[34]   J.-Y. Li, Y.-H. Li, M.-Y. Qi, Q. Lin, Z.-R. Tang, Y.-J. Xu, *ACS Catal.* **2020**, *10*, 6262.

[35]   J. Zhang, S. Wageh, A. Al-Ghamdi, J. Yu, *Appl. Catal. B* **2016**, *192*, 101.

[36]   K. Wu, T. Lian, *Chem. Soc. Rev.* **2016**, *45*, 3781.

[37]   O. Stroyuk, A. Raevskaya, N. Gaponik, *Chem. Soc. Rev.* **2018**, *47*, 5354.

[38]   C. O. Tuck, E. Pérez, I. T. Horváth, R. A. Sheldon, M. Poliakoff, *Science* **2012**, *337*, 695.

[39]   A. J. Ragauskas, G. T. Beckham, M. J. Biddy, R. Chandra, F. Chen, M. F. Davis, B. H. Davison, R. A. Dixon, P. Gilna, M. Keller, P. Langan, A. K. Naskar, J. N. Saddler, T. J. Tschaplinski, G. A. Tuskan, C. E. Wyman, *Science* **2014**, *344*, 1246843.

[40]   S. Van den Bosch, W. Schutyser, R. Vanholme, T. Driessen, S. F. Koelewijn, T. Renders, B. De Meester, W. J. J. Huijgen, W. Dehaen, C. M. Courtin, B. Lagrain, W. Boerjan, B. F. Sels, *Energy Environ. Sci.* **2015**, *8*, 1748.

[41]   Y. Liao, S.-F. Koelewijn, G. Van den Bossche, J. Van Aelst, S. Van den Bosch, T. Renders, K. Navare, T. Nicolaï, K. Van Aelst, M. Maesen, H. Matsushima, J. Thevelein, K. Van Acker, B. Lagrain, D. Verboekend, B. F. Sels, *Science* **2020**, *367*, 1385.

[42]   C. Li, X. Zhao, A. Wang, G. W. Huber, T. Zhang, *Chem. Rev.* **2015**, *115*, 11559.

[43]   R. Rinaldi, R. Jastrzebski, M. T. Clough, J. Ralph, M. Kennema, P. C. A. Bruijnincx, B. M. Weckhuysen, *Angew. Chem. Int. Ed.* **2016**, *55*, 8164.

[44]   L. Shuai, M. T. Amiri, Y. M. Questell-Santiago, F. Héroguel, Y. Li, H. Kim, R. Meilan, C. Chapple, J. Ralph, J. S. Luterbacher, *Science* **2016**, *354*, 329.

[45]   S. Kim, S. C. Chmely, M. R. Nimlos, Y. J. Bomble, T. D. Foust, R. S. Paton, G. T. Beckham, *J. Phys. Chem. Lett.* **2011**, *2*, 2846.

[46]   X. Wu, X. Fan, S. Xie, J. Lin, J. Cheng, Q. Zhang, L. Chen, Y. Wang, *Nat. Catal.* **2018**, *1*, 772.

[47]   A. Rahimi, A. Ulbrich, J. J. Coon, S. S. Stahl, *Nature* **2014**, *515*, 249.

[48]   C. S. Lancefield, O. S. Ojo, F. Tran, N. J. Westwood, *Angew. Chem. Int. Ed.* **2015**, *54*, 258.

[49]   J. D. Nguyen, B. S. Matsuura, C. R. J. Stephenson, *J. Am. Chem. Soc.* **2014**, *136*, 1218.

[50]   A. Das, B. König, *Green Chem.* **2018**, *20*, 4844.

[51]   N. Luo, M. Wang, H. Li, J. Zhang, T. Hou, H. Chen, X. Zhang, J. Lu, F. Wang, *ACS Catal.* **2017**, *7*, 4571.

[52]   G. Han, T. Yan, W. Zhang, Y. C. Zhang, D. Y. Lee, Z. Cao, Y. Sun, *ACS Catal.* **2019**, *9*, 11341.

[53]   C. Fabbri, M. Bietti, O. Lanzalunga, *J. Org. Chem.* **2005**, *70*, 2720.

[54]   P. H. Kandanarachchi, T. Autrey, J. A. Franz, *J. Org. Chem.* **2002**, *67*, 7937.

[55]   H. Yoo, M.-W. Lee, S. Lee, J. Lee, S. Cho, H. Lee, H. G. Cha, H. S. Kim, *ACS Catal.* **2020**, *10*, 8465.

[56]   K. Chen, J. Schwarz, T. A. Karl, A. Chatterjee, B. König, *Chem. Commun.* **2019**, *55*, 13144.

[57]   N. Kamimura, K. Takahashi, K. Mori, T. Araki, M. Fujita, Y. Higuchi, E. Masai, *Environ. Microbiol. Rep.* **2017**, *9*, 679.

[58]   W. S. Kontur, C. N. Olmsted, L. M. Yusko, A. V. Niles, K. A. Walters, E. T. Beebe, K. A. Vander Meulen, S. D. Karlen, D. L. Gall, D. R. Noguera, T. J. Donohue, *J. Biol. Chem.* **2019**, *294*, 1877.

[59]   G. E. Klinger, Y. Zhou, P. Hao, J. Robbins, J. M. Aquilina, J. E. Jackson, E. L. Hegg, *ChemSusChem* **2019**, *12*, 4775.

[60]   G. E. Klinger, Y. Zhou, J. A. Foote, A. M. Wester, Y. Cui, M. Alherech, S. S. Stahl, J. E. Jackson, E. L. Hegg, *ChemSusChem* **2020**, *13*, 4394.

[61]   S. Van den Bosch, T. Renders, S. Kennis, S. F. Koelewijn, G. Van den Bossche, T. Vangeel, A. Deneyer, D. Depuydt, C. M. Courtin, J. M. Thevelein, W. Schutyser, B. F. Sels, *Green Chem.* **2017**, *19*, 3313.

[62]   T. Renders, G. Van den Bossche, T. Vangeel, K. Van Aelst, B. Sels, *Curr. Opin. Biotechnol.* **2019**, *56*, 193.

[63]   S. Van den Bosch, S.-F. Koelewijn, T. Renders, G. Van den Bossche, T. Vangeel, W. Schutyser, B. F. Sels, in *Lignin Chemistry*, (Eds: L. Serrano, R. Luque, B. F. Sels), Springer International Publishing, Cham **2020**, 129.

[64]   X. Wu, S. Xie, C. Liu, C. Zhou, J. Lin, J. Kang, Q. Zhang, Z. Wang, Y. Wang, *ACS Catal.* **2019**, *9*, 8443.

[65]   D. W. Wakerley, M. F. Kuehnel, K. L. Orchard, K. H. Ly, T. E. Rosser, E. Reisner, *Nat. Energy* **2017**, *2*, 17021.

[66]   T. Uekert, F. Dorchies, C. M. Pichler, E. Reisner, *Green Chem.* **2020**, *22*, 3262.

[67]   H. Kasap, D. S. Achilleos, A. Huang, E. Reisner, *J. Am. Chem. Soc.* **2018**, *140*, 11604.

[68]   S. Chen, R. Wojcieszak, F. Dumeignil, E. Marceau, S. Royer, *Chem. Rev.* **2018**, *118*, 11023.

[69]   P. Gallezot, *Chem. Soc. Rev.* **2012**, *41*, 1538.

[70]   H. Zhang, S. Xie, J. Hu, X. Wu, Q. Zhang, J. Cheng, Y. Wang, *Chem. Commun.* **2020**, *56*, 1776.

[71]   S. Song, J. Qu, P. Han, M. J. Hülsey, G. Zhang, Y. Wang, S. Wang, D. Chen, J. Lu, N. Yan, *Nat. Commun.* **2020**, *11*, 4899.

[72]   T. Kawai, T. Sakata, *Nature* **1980**, *286*, 474.

[73]   X. Fu, J. Long, X. Wang, D. Y. C. Leung, Z. Ding, L. Wu, Z. Zhang, Z. Li, X. Fu, *Int. J. Hydrogen. Energ.* **2008**, *33*, 6484.

[74]   Y. Li, J. Wang, S. Peng, G. Lu, S. Li, *Int. J. Hydrogen. Energ.* **2010**, *35*, 7116.

[75]   J. C. Colmenares, A. Magdziarz, K. Kurzydlowski, J. Grzonka, O. Chernyayeva, D. Lisovytskiy, *Appl. Catal. B: Environ.* **2013**, *134*, 136.

[76]   S. Xu, P. Zhou, Z. Zhang, C. Yang, B. Zhang, K. Deng, S. Bottle, H. Zhu, *J. Am. Chem. Soc.* **2017**, *139*, 14775.

[77]   B. Zhou, J. Song, Z. Zhang, Z. Jiang, P. Zhang, B. Han, *Green Chem.* **2017**, *19*, 1075.

[78]   T. Simon, N. Bouchonville, M. J. Berr, A. Vaneski, A. Adrović, D. Volbers, R. Wyrwich, M. Döblinger, A. S. Susha, A. L. Rogach, F. Jäckel, J. K. Stolarczyk, J. Feldmann, *Nat. Mater.* **2014**, *13*, 1013.

[79]   G. Han, Y.-H. Jin, R. A. Burgess, N. E. Dickenson, X.-M. Cao, Y. Sun, *J. Am. Chem. Soc.* **2017**, *139*, 15584.

[80]   H.-F. Ye, R. Shi, X. Yang, W.-F. Fu, Y. Chen, *Appl. Catal. B: Environ.* **2018**, *233*, 70.

[81]   Y.-H. Li, F. Zhang, Y. Chen, J.-Y. Li, Y.-J. Xu, *Green Chem.* **2020**, *22*, 163.

[82]   N. C. Luo, T. Montini, J. Zhang, P. Fornasiero, E. Fonda, T. T. Hou, W. Nie, J. M. Lu, J. X. Liu, M. Heggen, L. Lin, C. T. Ma, M. Wang, F. T. Fan, S. Y. Jin, F. Wang, *Nat. Energy* **2019**, *4*, 575.

[83]   H. Zang, K. Wang, M. Zhang, R. Xie, L. Wang, E. Y. X. Chen, *Catal. Sci. Technol.* **2018**, *8*, 1777.

[84]   K. P. McClelland, E. A. Weiss, *ACS Appl. Energy Mater.* **2019**, *2*, 92.

[85]   N. Luo, T. Hou, S. Liu, B. Zeng, J. Lu, J. Zhang, H. Li, F. Wang, *ACS Catal.* **2019**, *10*, 762.

[86]   G. Han, X. Liu, Z. Cao, Y. Sun, *ACS Catal.* **2020**, *10*, 9346.

[87]   J. J. Bozell, G. R. Petersen, *Green Chem.* **2010**, *12*, 539.

[88]   M. Wang, M. Liu, J. Lu, F. Wang, *Nat. Commun.* **2020**, *11*, 1083.

[89]   S. Xie, Z. Shen, J. Deng, P. Guo, Q. Zhang, H. Zhang, C. Ma, Z. Jiang, J. Cheng, D. Deng, Y. Wang, *Nat. Commun.* **2018**, *9*, 1181.

[90]   H. Lu, J. Zhao, L. Li, L. Gong, J. Zheng, L. Zhang, Z. Wang, J. Zhang, Z. Zhu, *Energy Environ. Sci.* **2011**, *4*, 3384.

[91]   X. Wu, J. Li, S. Xie, P. Duan, H. Zhang, J. Feng, Q. Zhang, J. Cheng, Y. Wang, *Chem* **2020**, *11*, 3038.

[92]   F. Dénès, M. Pichowicz, G. Povie, P. Renaud, *Chem. Rev.* **2014**, *114*, 2587.

[93]   M. Chhowalla, H. S. Shin, G. Eda, L.-J. Li, K. P. Loh, H. Zhang, *Nat. Chem.* **2013**, *5*, 263.

[94]   K. A. Ubaid, X. Zhang, V. K. Sharma, L. Li, *Environ. Chem. Lett.* **2020**, *18*, 97.

[95]   J. Jasieniak, P. Mulvaney, *J. Am. Chem. Soc.* **2007**, *129*, 2841.

Xuejiao Wu received her B.S. degree (2015) from Xiamen University and obtained her Ph.D. degree (2020) from Xiamen University under the supervision of Prof. Ye Wang. She then carried out postdoctoral research at Prof. Bert F. Sels group at KU Leuven. Her research interest focuses on the valorization of lignocellulose, in particular by photocatalytic approaches.

Shunji Xie received his B. S. and M. Sc. degrees from Hunan University of China in 2008 and 2011, and obtained his Ph.D. degree from Xiamen University in 2014. He then carried out a postdoctoral research at the Collaborative Innovation Center of Chemistry for Energy Materials (*i*ChEM). He became full professor of Xiamen University in 2021. His research interest focuses on photocatalysis and electrocatalysis for C1 and sustainable chemistry, including CO_2 reduction, CH_4 oxidation, biomass conversion and ethylene glycol synthesis.

Bert F. Sels, currently full professor at KU Leuven, obtained his PhD degree in 2000 in the field of heterogeneous oxidation catalysis. He was awarded the DSM Chemistry Award in 2000, the Incentive Award by the Belgian Chemical Society in 2005 and the Green Chemistry Award in 2015. He is founder and head of the Centre for sustainable catalysis and engineering, designing heterogeneous catalysts for future challenges in industrial organic and environmental catalysis. His expertise includes heterogeneous catalysis in bio-refineries, design of hierarchical zeolites and carbons and the spectroscopic and kinetic study of active sites for small-molecule activation. He serves as associate editor of ACS Sustainable Chemistry and Engineering, and member of the European Academy of Sciences and Arts.

Ye Wang received his B.S. degree from Nanjing University and obtained his Ph.D. degree in 1996 from Tokyo Institute of Technology. He then worked at Tokyo Institute of Technology, Tohoku University and Hiroshima University, and was promoted to associate professor at Hiroshima University in 2001. He became full professor of Xiamen University in the August of 2001. He serves as associate editor of ACS Catalysis and council member of International Association of Catalysis Societies. The research interest of Prof. Ye Wang's group is catalysis for C1 and sustainable chemistry, including C−O/C−C cleavage chemistry for cellulose/lignin valorization, C−H activation and C−C coupling of C1 molecules.

The table of contents entry（50–60 words）:

The recent advances in metal sulfide-based photocatalytic systems for lignocellulose valorization are highlighted, with a focus on structure–performance analysis. The reaction mechanisms and the functions of metal sulfides are carefully examined. The unique abilities of metal sulfides in driving photocatalytic C−O bond cleavage, selective oxidations, C−C coupling and C−H activation are summarized and discussed to inspire future research efforts.

Metal Sulfide Photocatalysts for Lignocellulose Valorization

Xuejiao Wu, Shunji Xie,* Haikun Zhang, Qinghong Zhang, Bert F. Sels,* and Ye Wang*

TOC Figure: 55 mm broad × 50 mm high